Neoplasma 2025; 72(4): 275–285

doi:10.4149/neo_2025_250219N83

ELK1 modulates SF3B3 transcriptional activity to stimulate proliferation and inhibit apoptosis in gastric cancer through the activation of the MAPK pathway

Yaqing ZHANG[1,#], Lei GAO[1,#], Lixin LIU[2], Hao CHEN[1,3,4,*]

[1]The Second Hospital & Clinical Medical School, Lanzhou University, Lanzhou, Gansu, China; [2]Department of Thoracic Surgery, The First Hospital of Lanzhou University, Lanzhou, Gansu, China; [3]Department of Surgical Oncology, The Second Hospital & Clinical Medical School, Lanzhou University, Lanzhou, Gansu, China; [4]Gansu Provincial Key Laboratory of Environment Oncology, The Second Hospital & Clinical Medical School, Lanzhou University, Lanzhou, Gansu, China

**Correspondence: ery_chenh@lzu.edu.cn*
[#]Contributed equally to this work

Received February 19, 2025 / Accepted August 18, 2025

Gastric cancer (GC) ranks as the fifth most common malignancy globally. Aberrant alternative splicing is implicated in tumorigenesis and progression. SF3B3, a key subunit of the spliceosome complex, is closely linked to alternative splicing dysfunction when its expression is dysregulated. This study delved into SF3B3's role and mechanisms in GC, aiming to uncover novel precision treatment targets. Through TCGA database analysis, SF3B3 was found to be upregulated in GC tissues, associated with poor prognosis and immune infiltration. In vitro experiments included cell culture, transduction, CCK-8, colony formation, scratch, migration, apoptosis assays, cell cycle analysis, and western blot, demonstrating that SF3B3 knockdown curbed GC cell proliferation, migration, and invasion, induced apoptosis and cell cycle arrest, while its overexpression had opposite effects. In vivo xenograft experiments showed that SF3B3 suppression markedly inhibits tumor growth. Transcriptome analysis and western blot suggested that SF3B3 promotes GC cell proliferation and impedes apoptosis by activating the MAPK pathway. Moreover, transcription factor ELK1 was shown to regulate SF3B3 expression, with a significant positive correlation between them. Overall, SF3B3 likely drives GC progression via the ELK1-SF3B3-MAPK axis, representing a potential precision treatment target for GC.

Key words: gastric cancer; bioinformatics analysis; ELK1-SF3B3-MAPK signaling axis; proliferation; apoptosis

Gastric cancer (GC) is the fifth most common cancer worldwide and ranks third in cancer-related mortality [1]. The primary treatment for early GC is endoscopic resection, while non-early operable GC is treated with surgery combined with D2 lymph node dissection, and the combination of perioperative or adjuvant chemotherapy can significantly improve the survival rate of patients with stage IB or higher cancer. The treatment for advanced GC involves sequential chemotherapy regimens. Currently, targeted therapies have achieved better clinical outcomes [2, 3]. Despite this, the prognosis for GC treatment remains poor. Therefore, it is crucial to deeply understand the mechanisms of GC development, identify potential therapeutic targets or combined therapeutic targets, and provide patients with precise, personalized treatment.

It has been found that the dysregulation of alternative splicing (AS) has a profound impact on the occurrence, development, metastasis, and treatment response of cancer, which are key processes [4]. Abnormal AS is another cancer-driving mechanism in addition to genetic changes, leading to the translation of transcripts that produce unconventional and unannotated protein forms, thereby generating new antigens that provide new candidate targets for cancer immunotherapy [5, 6]. At the same time, in cancer, the protein diversity caused by abnormal AS may lead to the acquisition of new or altered functions in tumor cells, such as promoting cell proliferation, evading apoptosis and drug resistance, and enhancing invasive and metastatic abilities [7–9]. Therefore, AS may become an important target for cancer diagnosis, prognosis, and treatment. SF3B3 is a subunit of the splicing factor 3B complex (SF3B), which, together with SF3A and the 12S RNA unit, forms the U2 small nuclear ribonucleoprotein complex (U2 snRNP), a key nucleophile in the first transesterification reaction of the splicing reaction [10]. Multiple studies have found that SF3B3 promotes the occurrence and development of various cancers, including colon,

bladder, ovarian, breast, and liver cancer [11]. This study will predict the impact of SF3B3 on GC based on bioinformatics analysis and explore the upstream and downstream molecular mechanisms of SF3B3 in regulating GC at the cellular and animal levels, providing a molecular basis for finding targets for the treatment of GC.

Materials and methods

Materials. Fetal Bovine Serum (FBS, ExCell Bio, #FSP500); Matrigel Matrix (Corning, #356234); Poly-HEMA (Sigma Aldrich, Shanghai, #P3932); RIPA Lysis Buffer (Beyotime, #P0013B); CCK-8 (Servicebio, #G4103-1ML); Annexin V-APC/7-AAD Apoptosis Kit (Liankebio, #AP105); Cell Cycle Detection Kit (Liankebio, #CCS012); EdU (RIBOBIO, #C10310-2); SF3B3 shRNA and overexpression lentiviral vectors were constructed by Shanghai Genechem Co., Ltd.; Dual-Luciferase Reporter Vector (Promega, #E1910) was constructed by Suzhou Genepharma Co., Ltd..

Bioinformatics analysis. STAR-counts data for GC tumors were downloaded from TCGA database, and TPM-formatted data were extracted and normalized using log2(TPM+1). The expression differences of SF3B3 between normal and tumor groups were analyzed, and further, online prediction software (https://kmplot.com/analysis/) was utilized to analyze the differences in OS, FP, and FPS between the high and low expression groups of SF3B3.

Immune infiltration analysis. In this study, we aim to perform a correlation analysis between single gene expression and immune infiltration matrix data from TCGA pan-cancer dataset, with the results visualized through a heatmap. The statistical analysis will utilize Spearman correlation, while immune infiltration will be assessed using the ssGSEA algorithm from the R package GSVA (version 1.46.0) [12], leveraging the 24 immune cell markers to calculate immune infiltration levels for the corresponding cloud-based data [13]. Subsequently, we will perform a correlation analysis between single genes and immune infiltration data across the pan-cancer dataset, visualizing the results with a heatmap. For GC data from TCGA database, we will categorize the main variables based on high and low expression levels, selecting appropriate statistical methods based on the data format and characteristics (using the stats and car packages). Results will be visualized using the ggplot2 package. Finally, we will examine the correlations between data variables and visualize the results using ggplot2.

Cell culture. GES-1, MKN28, AGS, MKN-45, HGC-27, and SNU216 cell lines were purchased from Shanghai Fuheng Biological Co., Ltd. and cultured in RPMI-1640 complete medium, which was prepared with 10% FBS, 1% penicillin-streptomycin, and 89% RPMI-1640 basal medium, under conditions of 37 °C and 5% CO_2. All cell lines were authenticated using short tandem repeat (STR) profiling within the past 3 years. All experiments were performed with mycoplasma-free cells.

Cell transduction. Three shRNA lentiviral vectors targeting SF3B3 mRNA, an overexpression lentiviral vector for the SF3B3 gene, and an overexpression vector for the ELK1 gene were designed and synthesized by Shanghai Genechem Co., Ltd.. The recombinant lentiviral vectors were produced by co-transfecting GV112 vector plasmids carrying target sequences (GV112 for shRNA, GV208 for overexpression mRNA), Helper 1.0 plasmids, and Helper 2.0 plasmids into 293T cells using LipoFiterTM, resulting in lentiviral packaging. Successfully constructed lentiviral vectors were transduced into target cells with polybrene, whereas AGS and MKN45 cells were transduced with shRNA lentiviral vectors, and HGC27 cells were transduced with SF3B3 overexpression lentiviral vectors. Stable cells were selected with puromycin, and the knockdown and overexpression efficiencies were verified by western blot and qPCR.

CCK-8 assay. Cells in logarithmic growth phase were seeded at a density of 1.5×10^4 cells/well in a 96-well plate with 100 μl/well. After overnight incubation, 10 μl of CCK-8 solution was added to each well, and absorbance values (A) were measured at 450 nm at 24 h, 48 h, 72 h, and 96 h. Proliferation curves were plotted using the absorbance values.

Colony formation assay. Cells in logarithmic growth phase were prepared as single-cell suspensions in medium containing 10% FBS, and 500 cells were plated in each well of a 6-well plate with 2 ml/well. The cells were further cultured in a cell incubator for 14 days. After washing with PBS, the cells were fixed with 4% paraformaldehyde for 30 min, washed with PBS, and then stained with 1 ml of crystal violet dye for 10 min. After washing with PBS, the plates were photographed with a digital camera.

Scratch assay. A straight line was uniformly drawn on the back of a 6-well plate using a ruler and a marker. Cells were then added and cultured until they covered more than 80% of the bottom of the well. The line was scratched with a pipette tip aligned with the line on the back, and the cells were washed twice with PBS. Serum-free medium was added, and the plate was returned to a 37 °C, 5% CO_2 incubator for further culture. Photos were taken at 0 h and 24 h to compare the scratch healing ability of each group.

Migration assay. Cell suspensions were added to the upper chamber of Transwell plates, while 500 μl of medium containing 20% FBS was added to the lower chamber. The plates were incubated at 37 °C for 48 h. After incubation, the inserts were removed, and the cells on the upper side that did not invade were gently wiped off with a cotton swab. The cells were then stained with 0.1% crystal violet for 30 min, rinsed with PBS, and photographed under a microscope to count and compare the invasive capabilities of the cells in each group.

Annexin V-APC/7-AAD apoptosis detection assay. Both adherent cells and cells in the supernatant were collected, washed with PBS, and resuspended gently in 195 μl of Annexin V-APC binding buffer. Then, 5 μl of Annexin V-APC was added and mixed gently. Subsequently, 10 μl of

7-AAD staining solution was added, mixed gently, and the cells were incubated in the dark at room temperature for 20 min. The apoptosis rate of cells in each group was detected using a flow cytometer.

Cell cycle analysis. Adherent cells from each group were collected by trypsinization, centrifuged, and washed with PBS. Then, 1 ml of prechilled 70% ethanol was added, mixed, and fixed at 4 °C for 2 h. After centrifugation to remove the fixing solution, the cells were washed with PBS, and 500 µl of PI staining solution was added. The cells were incubated at 37 °C in the dark for 30 min, and the cell cycle was detected using a flow cytometer.

EdU staining. Cells were seeded at a density of 1.5×10^5/well in a 6-well plate with 2 ml/well. After 24 h of culture, EdU reagent was added at a ratio of 1:1,000 and incubated for 2 h. The cells were then fixed and permeabilized, and the Click reaction was used to label the cells with Apollo643-azide. The cell nuclei were stained with Hoechst 33342. Cells were observed and imaged under a fluorescence microscope.

Xenograft tumor experiment. Twenty SPF-grade female Balb/C nude mice (6–8 weeks old) were purchased from Chengdu Yao Kang Biotechnology Co., Ltd.. The animal experiments were approved by the Ethics Committee of the Second Hospital of Lanzhou University (Approval Number: D2024-412).

sh-Ctrl cells and sh-SF3B3#1 cells were inoculated at a dose of 1×10^7 cells/mouse under the armpit of Balb/C nude mice (n=6). After inoculation, the sh-Ctrl cell tumor was used as the control group, and tumor size was measured every 4 days using calipers to measure the longest and shortest diameters of the tumor. Tumor volume V was calculated as V = (a × b^2)/2, where a is the long axis and b is the short axis. After the intervention, the tumor blocks were excised, divided into two parts; one part was snap-frozen in liquid nitrogen, and the other part was fixed with 4% paraformaldehyde for H&E and IHC experiments.

Hematoxylin and Eosin (H&E) staining. Tumor tissues were processed into paraffin sections. The sections were deparaffinized in xylene twice and rehydrated through a graded alcohol series. They were then stained in hematoxylin for 10 min, rinsed in distilled water, differentiated in 0.5% hydrochloric acid-alcohol solution for 30 s, and rinsed in tap water twice for 5 min each. The sections were stained in eosin for 1 min, rinsed in tap water, dehydrated through a graded alcohol series, cleared in xylene, and mounted for photography and analysis.

Immunohistochemistry (IHC) staining. The GC tissue microarrays, including 96 cancer tissues and 84 adjacent tissues, were purchased from Shanghai Outdo Biotech Company (#HStmA180Su19) and deparaffinized in xylene twice and rehydrated through a graded alcohol series. Antigen retrieval was performed using microwave acid treatment. The sections were then treated with hydrogen peroxide to quench endogenous peroxidase activity, followed by blocking with goat serum. The primary antibody was incubated (1:200, Ki-67 antibody, #27309-1-AP, Proteintech; 1:200, SF3B3 antibody, #ab209402, Abcam) at 4 °C overnight, and the biotin-labeled secondary antibody was incubated at 37 °C for 2 h. The sections were then incubated with HRP-conjugated streptavidin for 30 min, and after DAB chromogen development, they were counterstained with hematoxylin, dehydrated through a graded alcohol series, cleared in xylene, and mounted with neutral resin for photography and analysis. Quantitative IHC scoring was performed using the Immunoreactive Score (IRS). IRS = staining intensity score × percentage of positive cells score. Staining intensity was graded as 0 (no staining, negative), 1 (pale yellow, weak), 2 (brownish yellow, moderate), or 3 (dark brown, strong). The percentage of positive tumor cells was classified into four categories: 1 (<25%), 2 (26–50%), 3 (51–75%), and 4 (>75%).

Ethical statements. All clinical tissue samples used in the article were obtained with informed consent from patients, and the study was approved by the Ethics Committee of Shanghai Outdo Biotech Company (Approval No.: YB M-05-02).

Transcriptome analysis. When shNC MKN45 cells and shSF3B3 MKN45 cells reached the logarithmic phase, cells were collected and subjected to RNA extraction, sample quality assessment, library construction, library quality assessment, and library sequencing to obtain raw transcriptome data. The raw transcriptome data were processed by removing adapters and filtering by length and quality to obtain full-length sequences. The full-length sequences were polished to obtain consensus sequences. The consensus sequences were deduplicated based on alignment results with the reference genome or constructed contigs. Deduplication was followed by transcript quantification analysis, differential transcript identification, functional annotation, enrichment analysis, and protein-protein interaction network analysis.

JASPAR online prediction. The Jaspar online prediction software (https://jaspar.elixir.no/) was used to predict the upstream transcription factors of the SF3B3 gene.

ChIP assay. Tumor cells were fixed with 1% paraformaldehyde at room temperature for 15 minutes. A final concentration of 0.125 M glycine was added to quench the crosslinking reaction. After rinsing with PBS, protease inhibitors were added, and cells were scraped off with a cell scraper, centrifuged, and resuspended in ChIP lysis buffer (750 µl/1×10^7 cells). The cells were placed on ice for 10 minutes and then sonicated to shear DNA into fragments with an average size of 200–750 bp. Immunoprecipitation of nuclear chromatin was performed using immunoglobulin G (IgG, #A7016, Beyotime), ELK1 Rabbit Polyclonal antibody (1:50, #27420-1-AP, Proteintech) and Protein A/G (#P2089, Beyotime). The promoter sequence of the SF3B3 gene was retrieved from NCBI, and online tools were used to predict the upstream trans-binding sites of transcription factors on the SF3B3 gene. Primers were designed based on the predicted binding site regions for qRT-PCR detection.

Detailed information on primer sequences is presented in Supplementary Table S1.

Dual luciferase reporter assay. Based on the binding sites of transcription factors on the SF3B3 gene promoter sequence, dual luciferase reporter vectors (wild-type and mutant) were constructed using pGL4.10 as the backbone. The predicted transcription factors were overexpressed using the pcDNA3.1 plasmid. The dual luciferase reporter vectors and overexpression plasmids were transfected into 293T cells. Luciferase activity (firefly and Renilla) in the transfected cells was detected using a dual luciferase activity assay kit, with the constitutively expressed Renilla luciferase vector as a reference to calculate the relative activity of firefly luciferase in each group.

Western blot assay. Total proteins from cells and tissues were extracted using RIPA lysis buffer, and protein concentrations were determined using the BCA method. Proteins were denatured by adding 5× loading buffer and heating in water at 100 °C. The proteins were then subjected to gel electrophoresis using SDS-PAGE, transferred to a membrane, and incubated with the primary antibody at 4 °C overnight: Cleaved Caspase 3 antibody (1:1,000; #9661, Cell Signaling Technology); Cleaved Caspase 7 antibody (1:1,000; #8438, Cell Signaling Technology); PCNA antibody (1:500; #GB12010-50, Servicebio); Cyclin D1 antibody (1:200; #ab16663, Abcam); Phospho-ERK1/2 antibody (1:1,000; #4307, Cell Signaling Technology); ERK1/2 antibody (1:1,000; #4695, Cell Signaling Technology); P38 antibody (1:1,000; #8690, Cell Signaling Technology); Phospho-P38 antibody (1:1,000; #4511, Cell Signaling Technology); SF3B3 antibody (1:2,000; #ab209402, abcam); β-actin antibody (1:20,000; #66009-1-Ig, Proteintech) overnight at 4 °C, followed by incubation with the secondary antibody at room temperature for 1 h. ECL luminescent solution was added, and the membrane was scanned using a scanner to analyze the OD values.

Statistical analysis. Data were analyzed using SPSS 26.0 statistical software. Quantitative data are expressed as the mean ± standard deviation ($\bar{x} \pm s$), and categorical data are expressed as percentages (%). All experiments were repeated at least 3 times. Comparisons between two groups were made using independent samples t-tests, while comparisons among multiple groups were made using one-way ANOVA. Post-hoc pairwise comparisons among groups were performed using the LSD-t test. A p-value <0.05 indicates a statistically significant difference.

Results

Expression of SF3B3 in GC and its impact on survival. This study analyzed the expression of SF3B3 in GC tissues using the online database TCGA (https://www.cancer.gov/ccg/research/genome-sequencing/tcga) and found that SF3B3 expression was significantly elevated ($p<0.001$) (Supplementary Figures S1A, S1B). Further online analysis using https://kmplot.com/analysis/ revealed that patients with high SF3B3 expression in GC had significantly lower first progression (FP) compared to those with low expression ($p<0.05$) (Supplementary Figure S1C). Additionally, tissue microarray confirmation showed that SF3B3 expression in GC was significantly higher than in adjacent non-cancerous tissues ($p<0.05$) (Supplementary Figures S1D–S1F), and analysis of follow-up data indicated that patients with high SF3B3 expression had a 1.69 times higher risk of mortality and significantly shorter survival time than those with low SF3B3 expression ($p<0.05$) (Supplementary Figure S1G).

The relationship between SF3B3 expression and immune infiltration. As depicted in Supplementary Figure S2A, SF3B3 expression plays a regulatory role in the immune microenvironment across various types of cancer. Specifically, in stomach adenocarcinoma (STAD), the expression levels of SF3B3 are significantly positively correlated with the infiltration of Th2 cells, T helper cells, and NK ^{CD56bright} cells ($p<0.05$). Conversely, SF3B3 expression is significantly negatively correlated with the infiltration of Tgd cells, Tfh cells, T cells, pDC cells, NK cells, mast cells, macrophages, iDC cells, DC cells, cytotoxic cells, CD8 T cells, and B cells ($p<0.05$). This study further evaluates the impact of SF3B3 on the tumor microenvironment, as shown in Supplementary Figure S2B, SF3B3 expression is significantly negatively correlated with the StromalScore, ImmuneScore, and ESTIMATEScore in GC ($p<0.05$). A comparative analysis of the enrichment of various immune cells in GC with high and low SF3B3 expression levels confirmed the results from Supplementary Figure S2A (Supplementary Figure S2C). Additionally, the correlation analysis between SF3B3 expression levels and the enrichment levels of immune cells in GC further validated the findings from Supplementary Figure S2A (Supplementary Figure S2D).

SF3B3 promotes the proliferation, migration, and invasion of GC. This study investigated the role of SF3B3 in inhibiting GC cells *in vitro*. To select appropriate cell lines, the expression of SF3B3 in five GC cell lines was detected. It was found that, compared with normal GES-1 cells, the expression of SF3B3 was significantly increased in AGS, MKN-45, HGC-27, and SNU216 cells, except for MKN28 cells ($p<0.05$), with the expression levels ranked from high to low as AGS, MKN-45, HGC-27, SNU216, and MKN28 cells (Figure 1A). Therefore, this study chose the AGS, MKN-45, and HGC-27 cell lines for subsequent experiments. By using shRNA lentiviral vector knockdown technology, two shRNAs targeting the expression of the SF3B3 gene were designed and transduced into the AGS and MKN-45 GC cell lines, while the lentiviral vector was used to transduce HGC-27 cells to achieve overexpression of SF3B3 (Supplementary Figure S3). It was found that knocking down the expression of the SF3B3 gene significantly inhibited the proliferation, colony formation, migration, and invasion capabilities of the AGS and MKN-45 cell lines (Figures 1B–1K). In contrast, overexpression of SF3B3 significantly enhanced the proliferation,

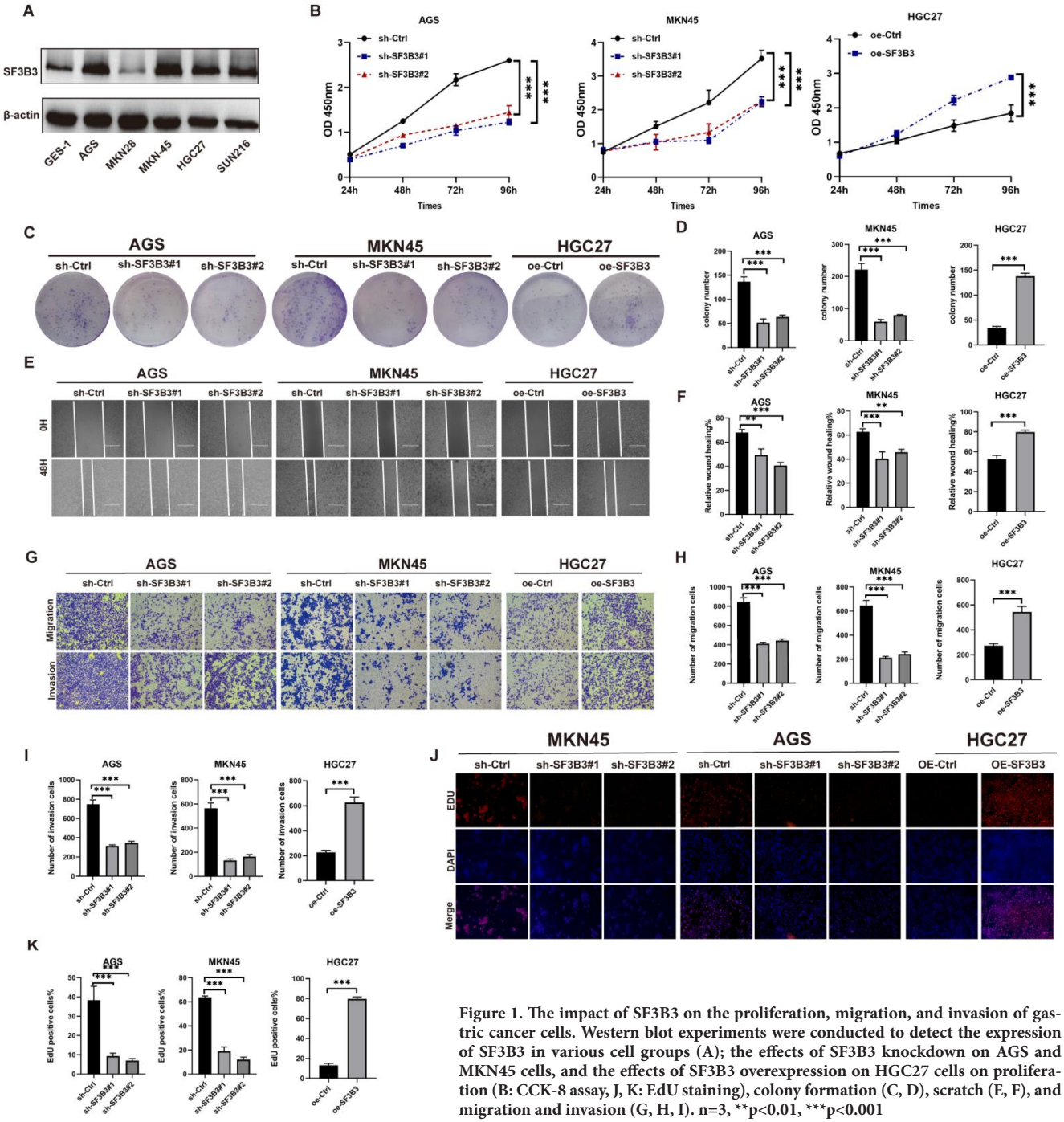

Figure 1. The impact of SF3B3 on the proliferation, migration, and invasion of gastric cancer cells. Western blot experiments were conducted to detect the expression of SF3B3 in various cell groups (A); the effects of SF3B3 knockdown on AGS and MKN45 cells, and the effects of SF3B3 overexpression on HGC27 cells on proliferation (B: CCK-8 assay, J, K: EdU staining), colony formation (C, D), scratch (E, F), and migration and invasion (G, H, I). n=3, **p<0.01, ***p<0.001

colony formation, migration, and invasion capabilities of HGC-27 cells (Figures 1B–1K).

SF3B3 inhibits apoptosis and cell cycle arrest of GC. This study found that knocking down the expression of the SF3B3 gene significantly induced significant apoptosis and cell cycle S phase arrest in the AGS and MKN-45 cell lines, promoted the activation of pro-apoptotic proteins Caspase 3 and Caspase 7, and inhibited the expression of proliferating cell nuclear antigen (PCNA), Cyclin D1, and Cyclin A (Figures 2A–2H). In contrast, overexpression of SF3B3 significantly suppressed cell apoptosis and cell cycle S phase arrest, prevented the activation of Caspase 3 and Caspase 7, and induced the expression of PCNA, Cyclin D1, and Cyclin A in the HGC-27 cells (Figures 2A–2H).

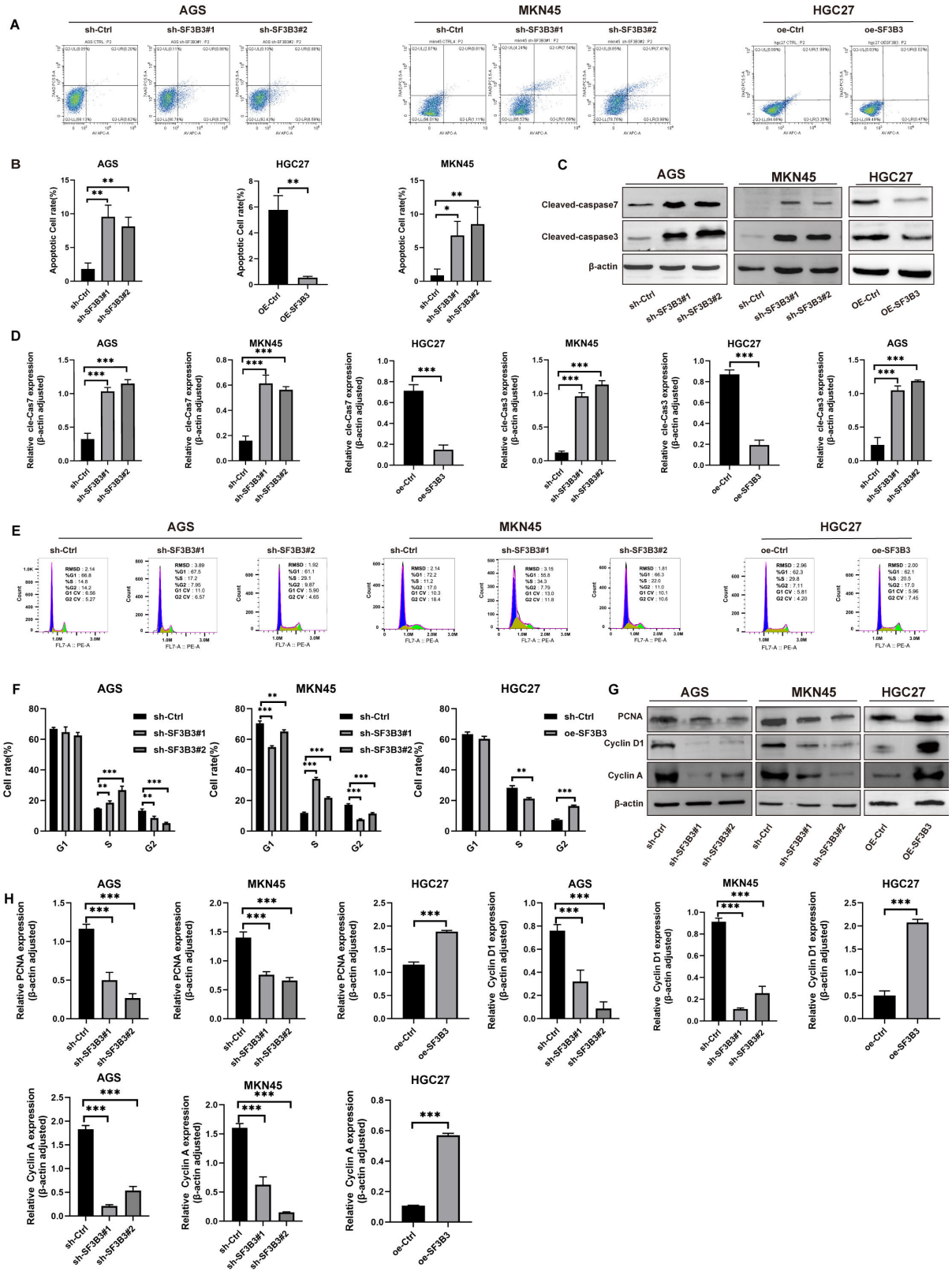

Figure 2. The impact of SF3B3 on the apoptosis and cell cycle of gastric cancer cells. The effects of SF3B3 knockdown on AGS and MKN45 cells, and the effects of SF3B3 overexpression on HGC27 cells on apoptosis (A, B: Annexin FITC/PI staining), apoptotic proteins (C, D: Western blot assay), cell cycle (E, F: PI staining), and cyclin proteins (G, H: Western blot assay). n=3, **p<0.01, ***p<0.001

SF3B3 promotes the growth of GC xenografts. To validate the role of SF3B3 in the development of GC, *in vivo* experiments were conducted, and it was found that the growth of GC xenografts was significantly inhibited after knockdown of SF3B3 ($p<0.05$) (Figures 3A–3C); pathological staining revealed that knockdown of SF3B3 reduced angiogenesis, decreased tumor cell numbers, and significantly lowered the expression of the cell proliferation marker protein Ki-67 in GC xenografts ($p<0.001$) (Figure 3D).

SF3B3 activates the ERK/MAPK P38 signaling pathway in GC cells. To further explore the downstream molecular mechanisms by which SF3B3 inhibits GC, this study conducted a transcriptome analysis of differentially expressed genes in MKN45 cells with SF3B3 knockdown (Figures 4A, 4B). The results revealed that the ERK/MAPK P38 signaling pathway was significantly inhibited in MKN45 cells with SF3B3 knockdown (Figures 4C, 4D), which was confirmed by western blot experiments. These experiments showed that after SF3B3 knockdown, the phosphorylation levels of ERK1/2 and P38 in AGS and MKN45 cells were significantly reduced, while the total protein levels remained unchanged. Conversely, after SF3B3 overexpression, the phosphorylation levels of ERK1/2 and P38 in HGC27 cells were significantly increased, while the total protein levels remained unchanged (Figures 4C, 4D).

ELK1 transcription factor regulates the expression of the SF3B3 gene. To explore the upstream regulatory mechanisms of the SF3B3 gene, this study analyzed the transcription factors of the SF3B3 gene in three online databases: AnimalTFDB, KnockTF, and JASPAR. The results revealed

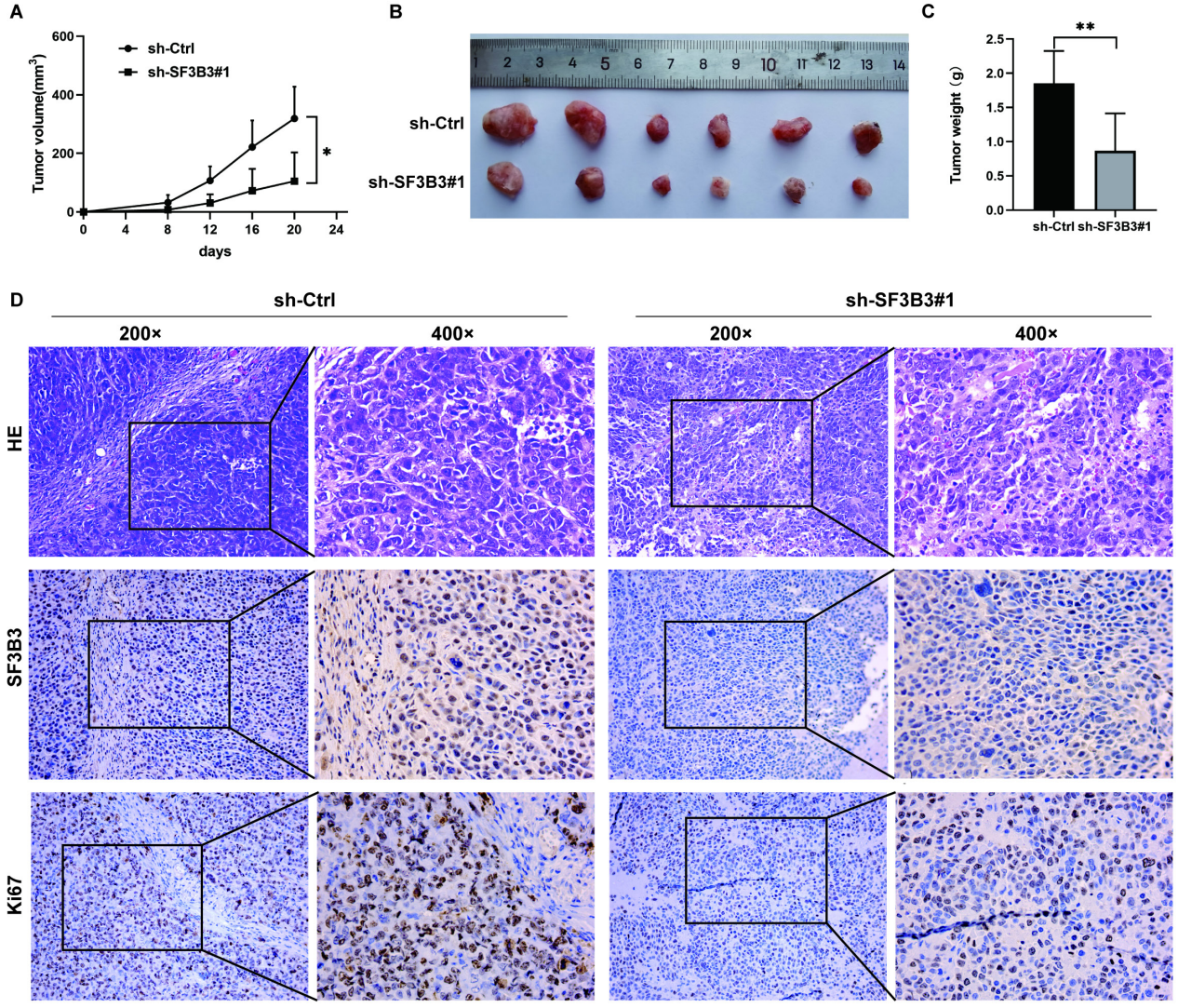

Figure 3. The impact of SF3B3 on the growth of gastric cancer xenografts. A) Morphological comparison of xenografts with knockdown of SF3B3 (sh-SF3B3) and controls (sh-Ctrl); B) Changes in xenograft volume; C) Changes in xenograft weight; D) H&E and immunohistochemical (SF3B3 and Ki-67 proteins) staining. n=6. **p<0.01

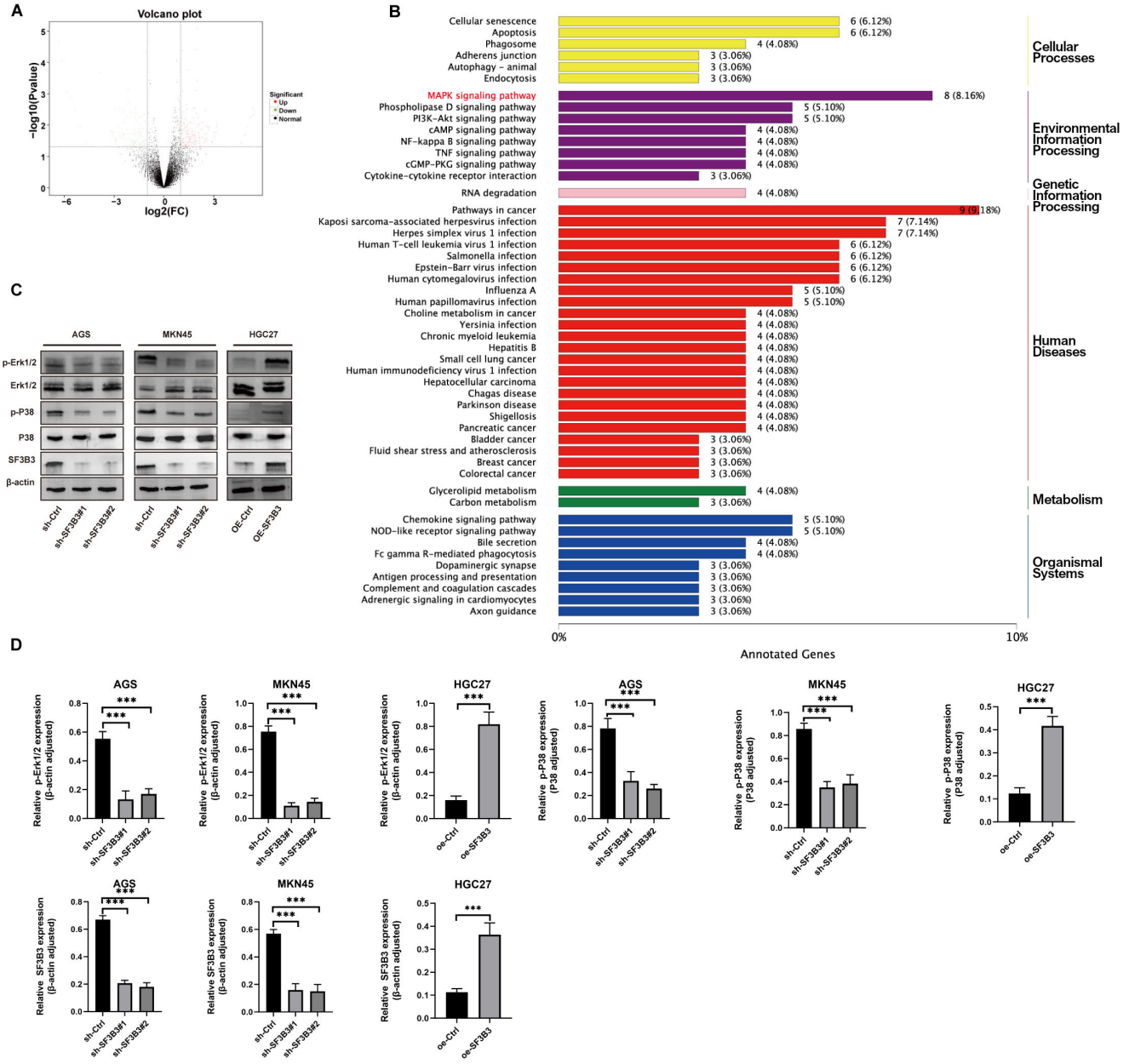

Figure 4. The impact of SF3B3 on the ERK/MAPK P38 signaling pathway in gastric cancer cells. A) Volcano plot of differentially expressed mRNA (transcriptome analysis); B) KEGG enrichment analysis of differential genes; C, D) Western blot experiments to detect proteins related to the ERK/MAPK P38 signaling pathway (C), and semi-quantitative analysis (D). n=3, ***p<0.001

that the transcription factor ELK1 could regulate the expression of the SF3B3 gene across all three databases (Figure 5A). Concurrently, online databases were utilized to discover a significant positive correlation between SF3B3 expression and ELK1 (Figure 5B). Overexpression of ELK1 in 293T and MKN45 cells significantly increased the expression of SF3B3 (Figure 5C, Supplementary Figure S4A). Furthermore, based on the predicted ELK1 binding to the P5 segment of the SF3B3 promoter sequence from the Jaspar database, ChIP experiments were conducted, which found that the P5 sequence could be significantly bound and precipitated by ELK1 in 293T and MKN45 cells (Figures 5D, 5E, Supplementary Figure S4B). A dual-luciferase reporter assay was performed using a construct with the P5 sequence, further confirming that ELK1 could significantly enhance the expression of firefly luciferase by binding to the P5 sequence in the promoter region of the SF3B3 gene in 293T and MKN45 cells (Figure 5F, Supplementary Figure S4C).

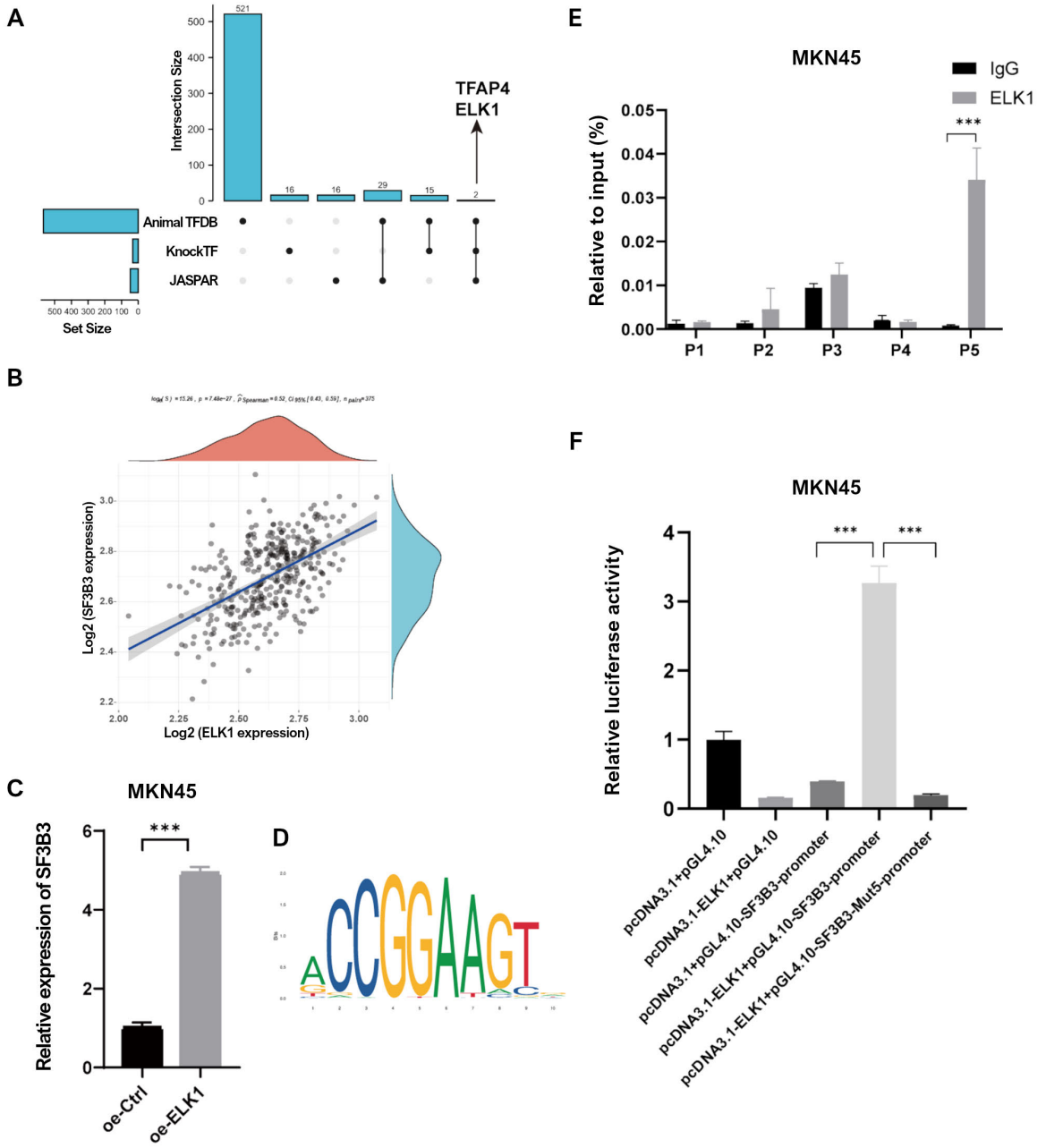

Figure 5. The regulatory effect of the ELK1 transcription factor on the expression of the SF3B3 gene. A) Analysis of transcription factors for the SF3B3 gene in the AnimalTFDB, KnockTF, and JASPAR online databases; B) Analysis of the correlation between SF3B3 and ELK1 expression using TCGA online database; C) qPCR detection of the effect of overexpressing ELK1 on SF3B3 expression in MKN45 cells; D) Prediction of the binding region P1-P5 of the transcription factor ELK1 on the SF3B3 gene promoter from the JASPAR database; E, F) ChIP (E) and dual-luciferase assay (F) to verify the binding region of ELK1 on the SF3B3 gene promoter. n=3, ***p<0.001

Discussion

RNA splicing is closely related to cell proliferation, survival, and differentiation, and is implicated in many human cancers. Studies have shown that in lymphoma, MYC can directly induce the transcription of snRNP genes and the arginine methyltransferase PRMT5, whose substrate is a component of the RNA splicing machinery [14, 15]. Several tumor suppressor genes, such as PTEN, ARID1A, and CDKN1A, are inactivated or downregulated at the transcriptional level due to aberrant AS, leading to the retention of introns [16, 17]. Additionally, aberrant AS in tumors can produce 12 protein isoforms of TP53, which are either inactivated due to intron retention or bind to different gene

promoters, leading to abnormal transcriptional regulation and promoting cellular transformation [18]. Therefore, elucidating the role of AS in cancer development is crucial for uncovering new targets for cancer therapy.

SF3B3 is a subunit of the splicing factor 3B complex (SF3B), which, together with SF3A and the 12S RNA unit, forms the U2 small nuclear ribonucleoprotein complex (U2 snRNP), a key nucleophile in the first transesterification reaction of the splicing reaction. Multiple studies have found that SF3B3 promotes the occurrence and development of various cancers, including colon, bladder, ovarian, breast, and liver cancer [18–21]. This study, through analysis of TCGA database, found that SF3B3 expression was significantly elevated in GC tissues, and patients with high SF3B3 expression had poorer prognosis, suggesting that SF3B3 may promote GC, potentially through aberrant high expression leading to dysregulation of AS. This finding is consistent with previous results, further confirming the important role of SF3B3 in GC. This study further reveals that SF3B3 is closely related to the immune microenvironment of GC. Its expression levels are significantly positively correlated with the infiltration of Th2 cells, T helper cells, and NK CD56 bright cells, and significantly negatively correlated with the infiltration of Tgd, TFH, T cells, pDC cells, NK cells, mast cells, macrophages, iDC cells, DC cells, cytotoxic cells, CD8 T cells, and B cells. These immune cells can interact with each other and synergistically promote the immune escape of GC. Immune escape can further promote the proliferation and metastasis of tumor cells. To this end, this study has verified the impact of SF3B3 on the proliferation, metastasis, and growth of GC *in vitro* and *in vivo* experiments. Further *in vitro* experiments revealed that knockdown of SF3B3 significantly inhibited the proliferation, colony formation, migration, and invasion of GC cells, while inducing apoptosis and cell cycle arrest. Interestingly, SF3B3 silencing in GC cells increased the S-phase fraction yet simultaneously reduced EdU fluorescence intensity. In normally proliferating cells, an expanded S-phase population typically signifies robust proliferation and thus higher EdU incorporation. Here, however, the S-phase accumulation resulted from S-phase arrest rather than accelerated progression, impairing DNA replication and consequently diminishing EdU incorporation during the last 2 h of cell cultivation. Consistent with this interpretation, Cyclin D1 and Cyclin A levels were downregulated in sh-SF3B3 cells. To validate this observation, dual-parameter flow cytometry combining Hoechst 33342 with EdU-Apollo643 will be performed in subsequent experiments. In contrast, overexpression of SF3B3 promoted these cellular behaviors, indicating that SF3B3 plays a significant role in promoting the proliferation and invasion of GC cells.

Current research on the downstream molecular mechanisms by which SF3B3 regulates cancer development is relatively clear, and it is based on the aberrant selective splicing of target genes by SF3B3 to promote carcinogenesis. In renal cancer, SF3B3 may have potential oncogenic effects through the selective splicing of EZH2 pre-mRNA [22]. In liver cancer, LINC01348 can prevent cancer cell metastasis by inhibiting SF3B3-mediated selective splicing of EZH2 pre-mRNA [19]. In colon cancer, SF3B3-mediated selective splicing of mTOR pre-mRNA promotes the progression and metastasis of rectal cancer [18]. This study found that SF3B3 can promote the proliferation and inhibit apoptosis of GC cells by activating the MAPK pathway, providing a new perspective on the role of SF3B3 in GC. However, whether it forms new structures of persistently activated MAPK proteins through selective splicing requires further investigation. Despite this, the mechanisms by which aberrant SF3B3 is regulated in cancer are unclear. As a culprit in the transformation of multiple genes into oncogenes, understanding the molecular mechanisms leading to its aberrance is of great significance. This study found that the ELK1 transcription factor can regulate the expression of SF3B3, and there is a significant positive correlation between SF3B3 and ELK1. Overexpression of ELK1 in 293T and MKN45 cells significantly increased the expression of SF3B3. This discovery reveals a new mechanism for the regulation of SF3B3 expression and provides a new molecular target for GC therapy.

In summary, this study not only confirms the important role of SF3B3 in GC but also reveals its molecular mechanisms in regulating GC proliferation and apoptosis, which may be closely related to the ELK1-SF3B3-MAPK signaling axis. This provides new targets for the precision treatment of GC and has the potential to improve the prognosis of GC patients. Future research can further explore the other functions and mechanisms of SF3B3 in GC, as well as the potential applications of the ELK1-SF3B3-MAPK signaling axis in GC therapy.

Supplementary information is available in the online version of the paper.

Acknowledgments: This work was supported by the National Natural Science Foundation of China (No. 82473266); Key Talents Project of Gansu Province (No. 2019RCXM020); Gansu Province Innovation Driven Assistance Project (No. GXH20230817-14); Cuiying Scientific and Technological Innovation Program of Lanzhou University Second Hospital (No. CY2023-ZD-01); Natural Science Foundation of Gansu province (No. 22JR5RA721).

References

[1] YANG WJ, ZHAO HP, YU Y, WANG JH, GUO L et al. Updates on global epidemiology, risk and prognostic factors of gastric cancer. World J Gastroenterol 2023; 29: 2452–2468. https://doi.org/10.3748/wjg.v29.i16.2452

[2] VINCZE Á. Endoscopic diagnosis and treatment in gastric cancer: Current evidence and new perspectives. Front Surg 2023; 10: 1122454. https://doi.org/10.3389/fsurg.2023.1122454

[3] SMYTH EC, NILSSON M, GRABSCH HI, VAN GRIEKEN NCT, LORDICK F. Gastric cancer. Lancet 2020; 396: 635–648. https://doi.org/10.1016/S0140-6736(20)31288-5

[4] ZHANG Y, QIAN J, GU C, YANG Y. Alternative splicing and cancer: a systematic review. Signal Transduct Target Ther 2021; 6: 78. https://doi.org/10.1038/s41392-021-00486-7

[5] WANG TY, LIU Q, REN Y, ALAM SK, WANG L et al. A pan-cancer transcriptome analysis of exitron splicing identifies novel cancer driver genes and neoepitopes. Mol Cell 2021; 81: 2246–2260.e2212. https://doi.org/10.1016/j.molcel.2021.03.028

[6] DENG K, YAO J, HUANG J, DING Y, ZUO J. Abnormal alternative splicing promotes tumor resistance in targeted therapy and immunotherapy. Transl Oncol 2021; 14: 101077. https://doi.org/10.1016/j.tranon.2021.101077

[7] SCIARRILLO R, WOJTUSZKIEWICZ A, ASSARAF YG, JANSEN G, KASPERS GJL et al. The role of alternative splicing in cancer: From oncogenesis to drug resistance. Drug Resist Updat 2020; 53: 100728. https://doi.org/10.1016/j.drup.2020.100728

[8] PENG Q, ZHOU Y, OYANG L, WU N, TANG Y et al. Impacts and mechanisms of alternative mRNA splicing in cancer metabolism, immune response, and therapeutics. Mol Ther 2022; 30: 1018–1035. https://doi.org/10.1016/j.ymthe.2021.11.010

[9] LI Y, DIAO Y, WANG Z, WANG S, PENG J et al. The splicing factor SF3B4 drives proliferation and invasion in cervical cancer by regulating SPAG5. Cell Death Discov 2022; 8: 326. https://doi.org/10.1038/s41420-022-01120-3

[10] SUN C. The SF3b complex: splicing and beyond. Cell Mol Life Sci 2020; 77: 3583–3595. https://doi.org/10.1007/s00018-020-03493-z

[11] GÖKMEN-POLAR Y, NEELAMRAJU Y, GOSWAMI CP, GU X, NALLAMOTHU G et al. Expression levels of SF3B3 correlate with prognosis and endocrine resistance in estrogen receptor-positive breast cancer. Mod Pathol 2015; 28: 677–685. https://doi.org/10.1038/modpathol.2014.146

[12] HÄNZELMANN S, CASTELO R, GUINNEY J. GSVA: gene set variation analysis for microarray and RNA-seq data. BMC Bioinformatics 2013; 14: 7. https://doi.org/10.1186/1471-2105-14-7

[13] BINDEA G, MLECNIK B, TOSOLINI M, KIRILOVSKY A, WALDNER M et al. Spatiotemporal dynamics of intratumoral immune cells reveal the immune landscape in human cancer. Immunity 2013; 39: 782–795. https://doi.org/10.1016/j.immuni.2013.10.003

[14] HODSON DJ, SCREEN M, TURNER M. RNA-binding proteins in hematopoiesis and hematological malignancy. Blood 2019; 133: 2365–2373. https://doi.org/10.1182/blood-2018-10-839985

[15] KOH CM, BEZZI M, LOW DHP, ANG WX, TEO SX et al. MYC regulates the core pre-mRNA splicing machinery as an essential step in lymphomagenesis. Nature 2015; 523: 96–100. https://doi.org/10.1038/nature14351

[16] LUO J, SOLIMINI NL, ELLEDGE SJ. Principles of cancer therapy: oncogene and non-oncogene addiction. Cell 2009; 136: 823–837. https://doi.org/10.1016/j.cell.2009.02.024

[17] TARN WY, STEITZ JA. A Novel Spliceosome Containing U11, U12, and U5 snRNPs Excises a Minor Class (AT–AC) Intron In Vitro. Cell 1996; 84: 801–811. https://doi.org/10.1016/S0092-8674(00)81057-0

[18] XU T, LI X, ZHAO W, WANG X, JIN L et al. SF3B3-regulated mTOR alternative splicing promotes colorectal cancer progression and metastasis. J Exp Clin Cancer Res 2024; 43: 126. https://doi.org/10.1186/s13046-024-03053-4

[19] LIN YH, WU MH, LIU YC, LYU PC, YEH CT et al. LINC01348 suppresses hepatocellular carcinoma metastasis through inhibition of SF3B3-mediated EZH2 pre-mRNA splicing. Oncogene 2021; 40: 4675–4685. https://doi.org/10.1038/s41388-021-01905-3

[20] ZHANG S, ZHANG J, AN Y, ZENG X, QIN Z et al. Multi-omics approaches identify SF3B3 and SIRT3 as candidate autophagic regulators and druggable targets in invasive breast carcinoma. Acta Pharm Sin B 2021; 11: 1227–1245. https://doi.org/10.1016/j.apsb.2020.12.013

[21] GÖKMEN-POLAR Y, NEELAMRAJU Y, GOSWAMI CP, GU X, NALLAMOTHU G et al. Expression levels of SF3B3 correlate with prognosis and endocrine resistance in estrogen receptor-positive breast cancer. Mod Pathol 2015; 28: 677–685. https://doi.org/10.1038/modpathol.2014.146

[22] CHEN K, XIAO H, ZENG J, YU G, ZHOU H et al. Alternative Splicing of EZH2 pre-mRNA by SF3B3 Contributes to the Tumorigenic Potential of Renal Cancer. Clin Cancer Res 2017; 23: 3428–3441. https://doi.org/10.1158/1078-0432.ccr-16-2020

Neoplasma 2025; 72(4): 275–285

doi:10.4149/neo_2025_250219N83

ELK1 modulates SF3B3 transcriptional activity to stimulate proliferation and inhibit apoptosis in gastric cancer through the activation of the MAPK pathway

Yaqing ZHANG[1,#], Lei GAO[1,#], Lixin LIU[2], Hao CHEN[1,3,4,*]

[1]The Second Hospital & Clinical Medical School, Lanzhou University, Lanzhou, Gansu, China; [2]Department of Thoracic Surgery, The First Hospital of Lanzhou University, Lanzhou, Gansu, China; [3]Department of Surgical Oncology, The Second Hospital & Clinical Medical School, Lanzhou University, Lanzhou, Gansu, China; [4]Gansu Provincial Key Laboratory of Environment Oncology, The Second Hospital & Clinical Medical School, Lanzhou University, Lanzhou, Gansu, China

**Correspondence: ery_chenh@lzu.edu.cn*
[#]Contributed equally to this work

Received February 19, 2025 / Accepted August 18, 2025

Gastric cancer (GC) ranks as the fifth most common malignancy globally. Aberrant alternative splicing is implicated in tumorigenesis and progression. SF3B3, a key subunit of the spliceosome complex, is closely linked to alternative splicing dysfunction when its expression is dysregulated. This study delved into SF3B3's role and mechanisms in GC, aiming to uncover novel precision treatment targets. Through TCGA database analysis, SF3B3 was found to be upregulated in GC tissues, associated with poor prognosis and immune infiltration. In vitro experiments included cell culture, transduction, CCK-8, colony formation, scratch, migration, apoptosis assays, cell cycle analysis, and western blot, demonstrating that SF3B3 knockdown curbed GC cell proliferation, migration, and invasion, induced apoptosis and cell cycle arrest, while its overexpression had opposite effects. In vivo xenograft experiments showed that SF3B3 suppression markedly inhibits tumor growth. Transcriptome analysis and western blot suggested that SF3B3 promotes GC cell proliferation and impedes apoptosis by activating the MAPK pathway. Moreover, transcription factor ELK1 was shown to regulate SF3B3 expression, with a significant positive correlation between them. Overall, SF3B3 likely drives GC progression via the ELK1-SF3B3-MAPK axis, representing a potential precision treatment target for GC.

Key words: gastric cancer; bioinformatics analysis; ELK1-SF3B3-MAPK signaling axis; proliferation; apoptosis

Gastric cancer (GC) is the fifth most common cancer worldwide and ranks third in cancer-related mortality [1]. The primary treatment for early GC is endoscopic resection, while non-early operable GC is treated with surgery combined with D2 lymph node dissection, and the combination of perioperative or adjuvant chemotherapy can significantly improve the survival rate of patients with stage IB or higher cancer. The treatment for advanced GC involves sequential chemotherapy regimens. Currently, targeted therapies have achieved better clinical outcomes [2, 3]. Despite this, the prognosis for GC treatment remains poor. Therefore, it is crucial to deeply understand the mechanisms of GC development, identify potential therapeutic targets or combined therapeutic targets, and provide patients with precise, personalized treatment.

It has been found that the dysregulation of alternative splicing (AS) has a profound impact on the occurrence, development, metastasis, and treatment response of cancer, which are key processes [4]. Abnormal AS is another cancer-driving mechanism in addition to genetic changes, leading to the translation of transcripts that produce unconventional and unannotated protein forms, thereby generating new antigens that provide new candidate targets for cancer immunotherapy [5, 6]. At the same time, in cancer, the protein diversity caused by abnormal AS may lead to the acquisition of new or altered functions in tumor cells, such as promoting cell proliferation, evading apoptosis and drug resistance, and enhancing invasive and metastatic abilities [7–9]. Therefore, AS may become an important target for cancer diagnosis, prognosis, and treatment. SF3B3 is a subunit of the splicing factor 3B complex (SF3B), which, together with SF3A and the 12S RNA unit, forms the U2 small nuclear ribonucleoprotein complex (U2 snRNP), a key nucleophile in the first transesterification reaction of the splicing reaction [10]. Multiple studies have found that SF3B3 promotes the occurrence and development of various cancers, including colon,

bladder, ovarian, breast, and liver cancer [11]. This study will predict the impact of SF3B3 on GC based on bioinformatics analysis and explore the upstream and downstream molecular mechanisms of SF3B3 in regulating GC at the cellular and animal levels, providing a molecular basis for finding targets for the treatment of GC.

Materials and methods

Materials. Fetal Bovine Serum (FBS, ExCell Bio, #FSP500); Matrigel Matrix (Corning, #356234); Poly-HEMA (Sigma Aldrich, Shanghai, #P3932); RIPA Lysis Buffer (Beyotime, #P0013B); CCK-8 (Servicebio, #G4103-1ML); Annexin V-APC/7-AAD Apoptosis Kit (Liankebio, #AP105); Cell Cycle Detection Kit (Liankebio, #CCS012); EdU (RIBOBIO, #C10310-2); SF3B3 shRNA and overexpression lentiviral vectors were constructed by Shanghai Genechem Co., Ltd.; Dual-Luciferase Reporter Vector (Promega, #E1910) was constructed by Suzhou Genepharma Co., Ltd..

Bioinformatics analysis. STAR-counts data for GC tumors were downloaded from TCGA database, and TPM-formatted data were extracted and normalized using log2(TPM+1). The expression differences of SF3B3 between normal and tumor groups were analyzed, and further, online prediction software (https://kmplot.com/analysis/) was utilized to analyze the differences in OS, FP, and FPS between the high and low expression groups of SF3B3.

Immune infiltration analysis. In this study, we aim to perform a correlation analysis between single gene expression and immune infiltration matrix data from TCGA pan-cancer dataset, with the results visualized through a heatmap. The statistical analysis will utilize Spearman correlation, while immune infiltration will be assessed using the ssGSEA algorithm from the R package GSVA (version 1.46.0) [12], leveraging the 24 immune cell markers to calculate immune infiltration levels for the corresponding cloud-based data [13]. Subsequently, we will perform a correlation analysis between single genes and immune infiltration data across the pan-cancer dataset, visualizing the results with a heatmap. For GC data from TCGA database, we will categorize the main variables based on high and low expression levels, selecting appropriate statistical methods based on the data format and characteristics (using the stats and car packages). Results will be visualized using the ggplot2 package. Finally, we will examine the correlations between data variables and visualize the results using ggplot2.

Cell culture. GES-1, MKN28, AGS, MKN-45, HGC-27, and SNU216 cell lines were purchased from Shanghai Fuheng Biological Co., Ltd. and cultured in RPMI-1640 complete medium, which was prepared with 10% FBS, 1% penicillin-streptomycin, and 89% RPMI-1640 basal medium, under conditions of 37 °C and 5% CO_2. All cell lines were authenticated using short tandem repeat (STR) profiling within the past 3 years. All experiments were performed with mycoplasma-free cells.

Cell transduction. Three shRNA lentiviral vectors targeting SF3B3 mRNA, an overexpression lentiviral vector for the SF3B3 gene, and an overexpression vector for the ELK1 gene were designed and synthesized by Shanghai Genechem Co., Ltd.. The recombinant lentiviral vectors were produced by co-transfecting GV112 vector plasmids carrying target sequences (GV112 for shRNA, GV208 for overexpression mRNA), Helper 1.0 plasmids, and Helper 2.0 plasmids into 293T cells using LipoFiterTM, resulting in lentiviral packaging. Successfully constructed lentiviral vectors were transduced into target cells with polybrene, whereas AGS and MKN45 cells were transduced with shRNA lentiviral vectors, and HGC27 cells were transduced with SF3B3 overexpression lentiviral vectors. Stable cells were selected with puromycin, and the knockdown and overexpression efficiencies were verified by western blot and qPCR.

CCK-8 assay. Cells in logarithmic growth phase were seeded at a density of 1.5×10^4 cells/well in a 96-well plate with 100 μl/well. After overnight incubation, 10 μl of CCK-8 solution was added to each well, and absorbance values (A) were measured at 450 nm at 24 h, 48 h, 72 h, and 96 h. Proliferation curves were plotted using the absorbance values.

Colony formation assay. Cells in logarithmic growth phase were prepared as single-cell suspensions in medium containing 10% FBS, and 500 cells were plated in each well of a 6-well plate with 2 ml/well. The cells were further cultured in a cell incubator for 14 days. After washing with PBS, the cells were fixed with 4% paraformaldehyde for 30 min, washed with PBS, and then stained with 1 ml of crystal violet dye for 10 min. After washing with PBS, the plates were photographed with a digital camera.

Scratch assay. A straight line was uniformly drawn on the back of a 6-well plate using a ruler and a marker. Cells were then added and cultured until they covered more than 80% of the bottom of the well. The line was scratched with a pipette tip aligned with the line on the back, and the cells were washed twice with PBS. Serum-free medium was added, and the plate was returned to a 37 °C, 5% CO_2 incubator for further culture. Photos were taken at 0 h and 24 h to compare the scratch healing ability of each group.

Migration assay. Cell suspensions were added to the upper chamber of Transwell plates, while 500 μl of medium containing 20% FBS was added to the lower chamber. The plates were incubated at 37 °C for 48 h. After incubation, the inserts were removed, and the cells on the upper side that did not invade were gently wiped off with a cotton swab. The cells were then stained with 0.1% crystal violet for 30 min, rinsed with PBS, and photographed under a microscope to count and compare the invasive capabilities of the cells in each group.

Annexin V-APC/7-AAD apoptosis detection assay. Both adherent cells and cells in the supernatant were collected, washed with PBS, and resuspended gently in 195 μl of Annexin V-APC binding buffer. Then, 5 μl of Annexin V-APC was added and mixed gently. Subsequently, 10 μl of

7-AAD staining solution was added, mixed gently, and the cells were incubated in the dark at room temperature for 20 min. The apoptosis rate of cells in each group was detected using a flow cytometer.

Cell cycle analysis. Adherent cells from each group were collected by trypsinization, centrifuged, and washed with PBS. Then, 1 ml of prechilled 70% ethanol was added, mixed, and fixed at 4 °C for 2 h. After centrifugation to remove the fixing solution, the cells were washed with PBS, and 500 µl of PI staining solution was added. The cells were incubated at 37 °C in the dark for 30 min, and the cell cycle was detected using a flow cytometer.

EdU staining. Cells were seeded at a density of 1.5×10^5/well in a 6-well plate with 2 ml/well. After 24 h of culture, EdU reagent was added at a ratio of 1:1,000 and incubated for 2 h. The cells were then fixed and permeabilized, and the Click reaction was used to label the cells with Apollo643-azide. The cell nuclei were stained with Hoechst 33342. Cells were observed and imaged under a fluorescence microscope.

Xenograft tumor experiment. Twenty SPF-grade female Balb/C nude mice (6–8 weeks old) were purchased from Chengdu Yao Kang Biotechnology Co., Ltd.. The animal experiments were approved by the Ethics Committee of the Second Hospital of Lanzhou University (Approval Number: D2024-412).

sh-Ctrl cells and sh-SF3B3#1 cells were inoculated at a dose of 1×10^7 cells/mouse under the armpit of Balb/C nude mice (n=6). After inoculation, the sh-Ctrl cell tumor was used as the control group, and tumor size was measured every 4 days using calipers to measure the longest and shortest diameters of the tumor. Tumor volume V was calculated as V = (a × b^2)/2, where a is the long axis and b is the short axis. After the intervention, the tumor blocks were excised, divided into two parts; one part was snap-frozen in liquid nitrogen, and the other part was fixed with 4% paraformaldehyde for H&E and IHC experiments.

Hematoxylin and Eosin (H&E) staining. Tumor tissues were processed into paraffin sections. The sections were deparaffinized in xylene twice and rehydrated through a graded alcohol series. They were then stained in hematoxylin for 10 min, rinsed in distilled water, differentiated in 0.5% hydrochloric acid-alcohol solution for 30 s, and rinsed in tap water twice for 5 min each. The sections were stained in eosin for 1 min, rinsed in tap water, dehydrated through a graded alcohol series, cleared in xylene, and mounted for photography and analysis.

Immunohistochemistry (IHC) staining. The GC tissue microarrays, including 96 cancer tissues and 84 adjacent tissues, were purchased from Shanghai Outdo Biotech Company (#HStmA180Su19) and deparaffinized in xylene twice and rehydrated through a graded alcohol series. Antigen retrieval was performed using microwave acid treatment. The sections were then treated with hydrogen peroxide to quench endogenous peroxidase activity, followed by blocking with goat serum. The primary antibody was incubated (1:200, Ki-67 antibody, #27309-1-AP, Proteintech; 1:200, SF3B3 antibody, #ab209402, Abcam) at 4 °C overnight, and the biotin-labeled secondary antibody was incubated at 37 °C for 2 h. The sections were then incubated with HRP-conjugated streptavidin for 30 min, and after DAB chromogen development, they were counterstained with hematoxylin, dehydrated through a graded alcohol series, cleared in xylene, and mounted with neutral resin for photography and analysis. Quantitative IHC scoring was performed using the Immunoreactive Score (IRS). IRS = staining intensity score × percentage of positive cells score. Staining intensity was graded as 0 (no staining, negative), 1 (pale yellow, weak), 2 (brownish yellow, moderate), or 3 (dark brown, strong). The percentage of positive tumor cells was classified into four categories: 1 (<25%), 2 (26–50%), 3 (51–75%), and 4 (>75%).

Ethical statements. All clinical tissue samples used in the article were obtained with informed consent from patients, and the study was approved by the Ethics Committee of Shanghai Outdo Biotech Company (Approval No.: YB M-05-02).

Transcriptome analysis. When shNC MKN45 cells and shSF3B3 MKN45 cells reached the logarithmic phase, cells were collected and subjected to RNA extraction, sample quality assessment, library construction, library quality assessment, and library sequencing to obtain raw transcriptome data. The raw transcriptome data were processed by removing adapters and filtering by length and quality to obtain full-length sequences. The full-length sequences were polished to obtain consensus sequences. The consensus sequences were deduplicated based on alignment results with the reference genome or constructed contigs. Deduplication was followed by transcript quantification analysis, differential transcript identification, functional annotation, enrichment analysis, and protein-protein interaction network analysis.

JASPAR online prediction. The Jaspar online prediction software (https://jaspar.elixir.no/) was used to predict the upstream transcription factors of the SF3B3 gene.

ChIP assay. Tumor cells were fixed with 1% paraformaldehyde at room temperature for 15 minutes. A final concentration of 0.125 M glycine was added to quench the crosslinking reaction. After rinsing with PBS, protease inhibitors were added, and cells were scraped off with a cell scraper, centrifuged, and resuspended in ChIP lysis buffer (750 µl/1×10^7 cells). The cells were placed on ice for 10 minutes and then sonicated to shear DNA into fragments with an average size of 200–750 bp. Immunoprecipitation of nuclear chromatin was performed using immunoglobulin G (IgG, #A7016, Beyotime), ELK1 Rabbit Polyclonal antibody (1:50, #27420-1-AP, Proteintech) and Protein A/G (#P2089, Beyotime). The promoter sequence of the SF3B3 gene was retrieved from NCBI, and online tools were used to predict the upstream trans-binding sites of transcription factors on the SF3B3 gene. Primers were designed based on the predicted binding site regions for qRT-PCR detection.

Detailed information on primer sequences is presented in Supplementary Table S1.

Dual luciferase reporter assay. Based on the binding sites of transcription factors on the SF3B3 gene promoter sequence, dual luciferase reporter vectors (wild-type and mutant) were constructed using pGL4.10 as the backbone. The predicted transcription factors were overexpressed using the pcDNA3.1 plasmid. The dual luciferase reporter vectors and overexpression plasmids were transfected into 293T cells. Luciferase activity (firefly and Renilla) in the transfected cells was detected using a dual luciferase activity assay kit, with the constitutively expressed Renilla luciferase vector as a reference to calculate the relative activity of firefly luciferase in each group.

Western blot assay. Total proteins from cells and tissues were extracted using RIPA lysis buffer, and protein concentrations were determined using the BCA method. Proteins were denatured by adding 5× loading buffer and heating in water at 100 °C. The proteins were then subjected to gel electrophoresis using SDS-PAGE, transferred to a membrane, and incubated with the primary antibody at 4 °C overnight: Cleaved Caspase 3 antibody (1:1,000; #9661, Cell Signaling Technology); Cleaved Caspase 7 antibody (1:1,000; #8438, Cell Signaling Technology); PCNA antibody (1:500; #GB12010-50, Servicebio); Cyclin D1 antibody (1:200; #ab16663, Abcam); Phospho-ERK1/2 antibody (1:1,000; #4307, Cell Signaling Technology); ERK1/2 antibody (1:1,000; #4695, Cell Signaling Technology); P38 antibody (1:1,000; #8690, Cell Signaling Technology); Phospho-P38 antibody (1:1,000; #4511, Cell Signaling Technology); SF3B3 antibody (1:2,000; #ab209402, abcam); β-actin antibody (1:20,000; #66009-1-Ig, Proteintech) overnight at 4 °C, followed by incubation with the secondary antibody at room temperature for 1 h. ECL luminescent solution was added, and the membrane was scanned using a scanner to analyze the OD values.

Statistical analysis. Data were analyzed using SPSS 26.0 statistical software. Quantitative data are expressed as the mean ± standard deviation ($\bar{x} \pm s$), and categorical data are expressed as percentages (%). All experiments were repeated at least 3 times. Comparisons between two groups were made using independent samples t-tests, while comparisons among multiple groups were made using one-way ANOVA. Post-hoc pairwise comparisons among groups were performed using the LSD-t test. A p-value <0.05 indicates a statistically significant difference.

Results

Expression of SF3B3 in GC and its impact on survival. This study analyzed the expression of SF3B3 in GC tissues using the online database TCGA (https://www.cancer.gov/ccg/research/genome-sequencing/tcga) and found that SF3B3 expression was significantly elevated ($p<0.001$) (Supplementary Figures S1A, S1B). Further online analysis using https://kmplot.com/analysis/ revealed that patients with high SF3B3 expression in GC had significantly lower first progression (FP) compared to those with low expression ($p<0.05$) (Supplementary Figure S1C). Additionally, tissue microarray confirmation showed that SF3B3 expression in GC was significantly higher than in adjacent non-cancerous tissues ($p<0.05$) (Supplementary Figures S1D–S1F), and analysis of follow-up data indicated that patients with high SF3B3 expression had a 1.69 times higher risk of mortality and significantly shorter survival time than those with low SF3B3 expression ($p<0.05$) (Supplementary Figure S1G).

The relationship between SF3B3 expression and immune infiltration. As depicted in Supplementary Figure S2A, SF3B3 expression plays a regulatory role in the immune microenvironment across various types of cancer. Specifically, in stomach adenocarcinoma (STAD), the expression levels of SF3B3 are significantly positively correlated with the infiltration of Th2 cells, T helper cells, and NK ^{CD56bright} cells ($p<0.05$). Conversely, SF3B3 expression is significantly negatively correlated with the infiltration of Tgd cells, Tfh cells, T cells, pDC cells, NK cells, mast cells, macrophages, iDC cells, DC cells, cytotoxic cells, CD8 T cells, and B cells ($p<0.05$). This study further evaluates the impact of SF3B3 on the tumor microenvironment, as shown in Supplementary Figure S2B, SF3B3 expression is significantly negatively correlated with the StromalScore, ImmuneScore, and ESTIMATEScore in GC ($p<0.05$). A comparative analysis of the enrichment of various immune cells in GC with high and low SF3B3 expression levels confirmed the results from Supplementary Figure S2A (Supplementary Figure S2C). Additionally, the correlation analysis between SF3B3 expression levels and the enrichment levels of immune cells in GC further validated the findings from Supplementary Figure S2A (Supplementary Figure S2D).

SF3B3 promotes the proliferation, migration, and invasion of GC. This study investigated the role of SF3B3 in inhibiting GC cells *in vitro*. To select appropriate cell lines, the expression of SF3B3 in five GC cell lines was detected. It was found that, compared with normal GES-1 cells, the expression of SF3B3 was significantly increased in AGS, MKN-45, HGC-27, and SNU216 cells, except for MKN28 cells ($p<0.05$), with the expression levels ranked from high to low as AGS, MKN-45, HGC-27, SNU216, and MKN28 cells (Figure 1A). Therefore, this study chose the AGS, MKN-45, and HGC-27 cell lines for subsequent experiments. By using shRNA lentiviral vector knockdown technology, two shRNAs targeting the expression of the SF3B3 gene were designed and transduced into the AGS and MKN-45 GC cell lines, while the lentiviral vector was used to transduce HGC-27 cells to achieve overexpression of SF3B3 (Supplementary Figure S3). It was found that knocking down the expression of the SF3B3 gene significantly inhibited the proliferation, colony formation, migration, and invasion capabilities of the AGS and MKN-45 cell lines (Figures 1B–1K). In contrast, overexpression of SF3B3 significantly enhanced the proliferation,

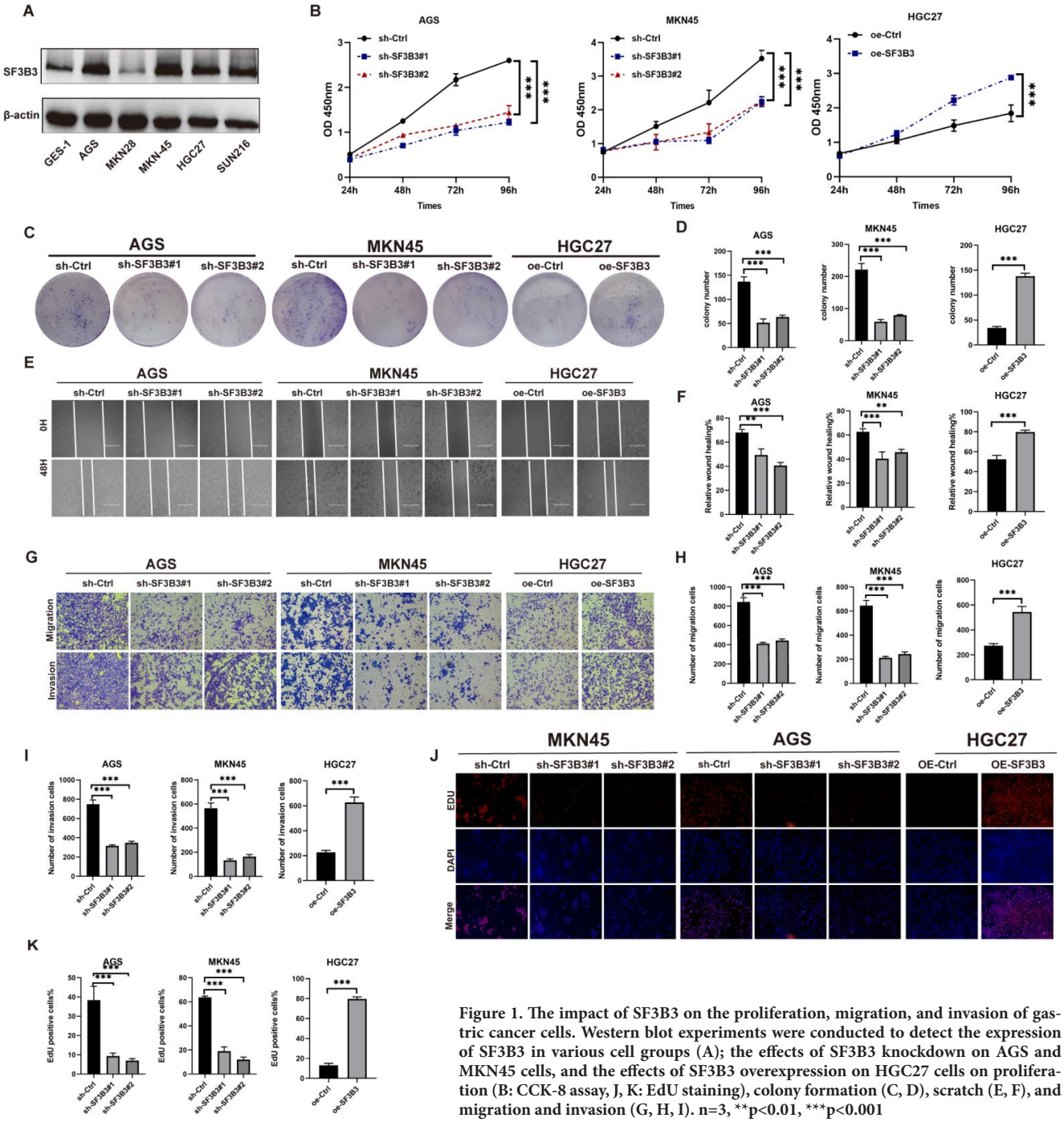

Figure 1. The impact of SF3B3 on the proliferation, migration, and invasion of gastric cancer cells. Western blot experiments were conducted to detect the expression of SF3B3 in various cell groups (A); the effects of SF3B3 knockdown on AGS and MKN45 cells, and the effects of SF3B3 overexpression on HGC27 cells on proliferation (B: CCK-8 assay, J, K: EdU staining), colony formation (C, D), scratch (E, F), and migration and invasion (G, H, I). n=3, **p<0.01, ***p<0.001

colony formation, migration, and invasion capabilities of HGC-27 cells (Figures 1B–1K).

SF3B3 inhibits apoptosis and cell cycle arrest of GC. This study found that knocking down the expression of the SF3B3 gene significantly induced significant apoptosis and cell cycle S phase arrest in the AGS and MKN-45 cell lines, promoted the activation of pro-apoptotic proteins Caspase 3 and Caspase 7, and inhibited the expression of proliferating cell nuclear antigen (PCNA), Cyclin D1, and Cyclin A (Figures 2A–2H). In contrast, overexpression of SF3B3 significantly suppressed cell apoptosis and cell cycle S phase arrest, prevented the activation of Caspase 3 and Caspase 7, and induced the expression of PCNA, Cyclin D1, and Cyclin A in the HGC-27 cells (Figures 2A–2H).

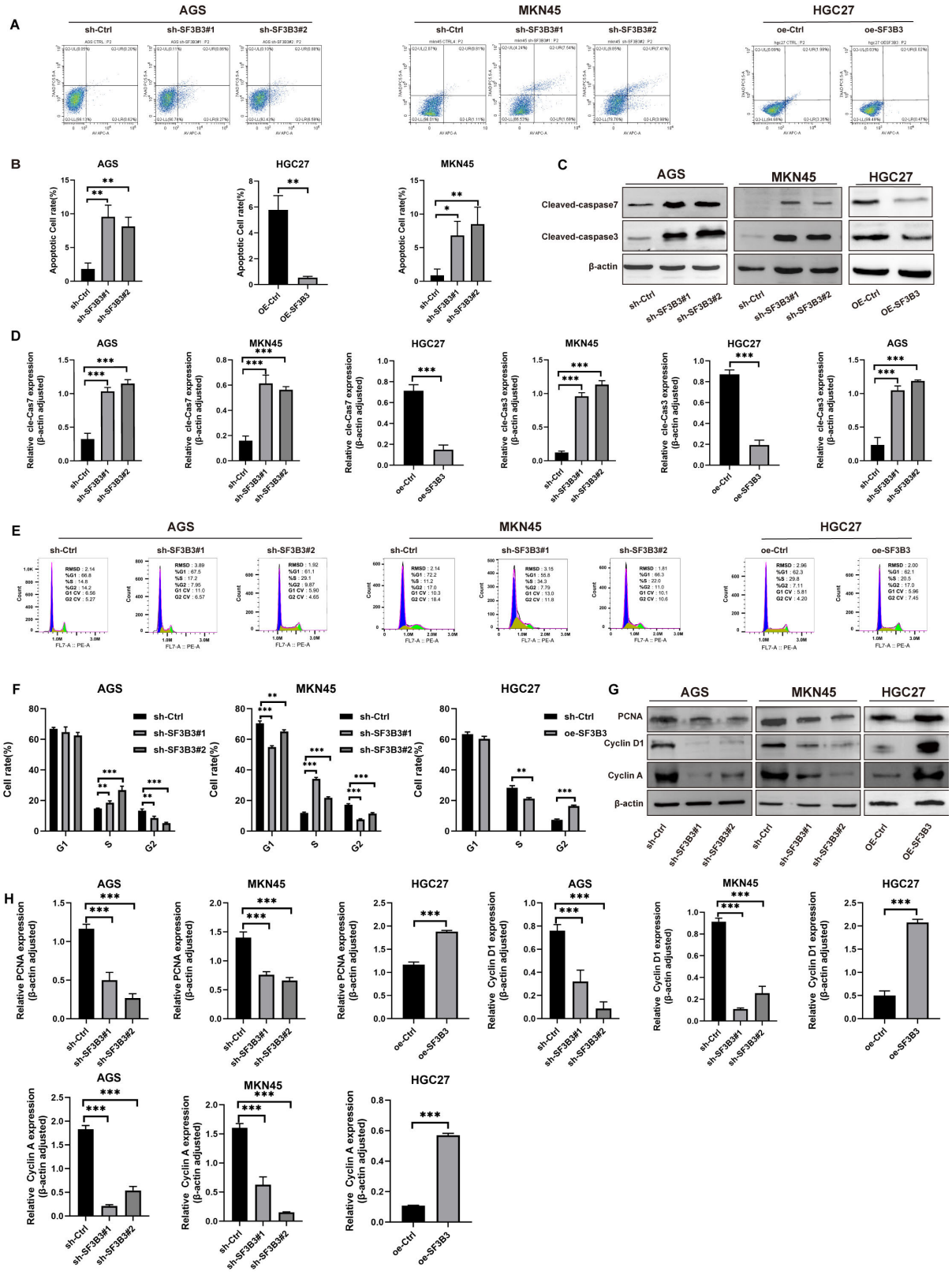

Figure 2. The impact of SF3B3 on the apoptosis and cell cycle of gastric cancer cells. The effects of SF3B3 knockdown on AGS and MKN45 cells, and the effects of SF3B3 overexpression on HGC27 cells on apoptosis (A, B: Annexin FITC/PI staining), apoptotic proteins (C, D: Western blot assay), cell cycle (E, F: PI staining), and cyclin proteins (G, H: Western blot assay). n=3, **p<0.01, ***p<0.001

SF3B3 promotes the growth of GC xenografts. To validate the role of SF3B3 in the development of GC, *in vivo* experiments were conducted, and it was found that the growth of GC xenografts was significantly inhibited after knockdown of SF3B3 ($p<0.05$) (Figures 3A–3C); pathological staining revealed that knockdown of SF3B3 reduced angiogenesis, decreased tumor cell numbers, and significantly lowered the expression of the cell proliferation marker protein Ki-67 in GC xenografts ($p<0.001$) (Figure 3D).

SF3B3 activates the ERK/MAPK P38 signaling pathway in GC cells. To further explore the downstream molecular mechanisms by which SF3B3 inhibits GC, this study conducted a transcriptome analysis of differentially expressed genes in MKN45 cells with SF3B3 knockdown (Figures 4A, 4B). The results revealed that the ERK/MAPK P38 signaling pathway was significantly inhibited in MKN45 cells with SF3B3 knockdown (Figures 4C, 4D), which was confirmed by western blot experiments. These experiments showed that after SF3B3 knockdown, the phosphorylation levels of ERK1/2 and P38 in AGS and MKN45 cells were significantly reduced, while the total protein levels remained unchanged. Conversely, after SF3B3 overexpression, the phosphorylation levels of ERK1/2 and P38 in HGC27 cells were significantly increased, while the total protein levels remained unchanged (Figures 4C, 4D).

ELK1 transcription factor regulates the expression of the SF3B3 gene. To explore the upstream regulatory mechanisms of the SF3B3 gene, this study analyzed the transcription factors of the SF3B3 gene in three online databases: AnimalTFDB, KnockTF, and JASPAR. The results revealed

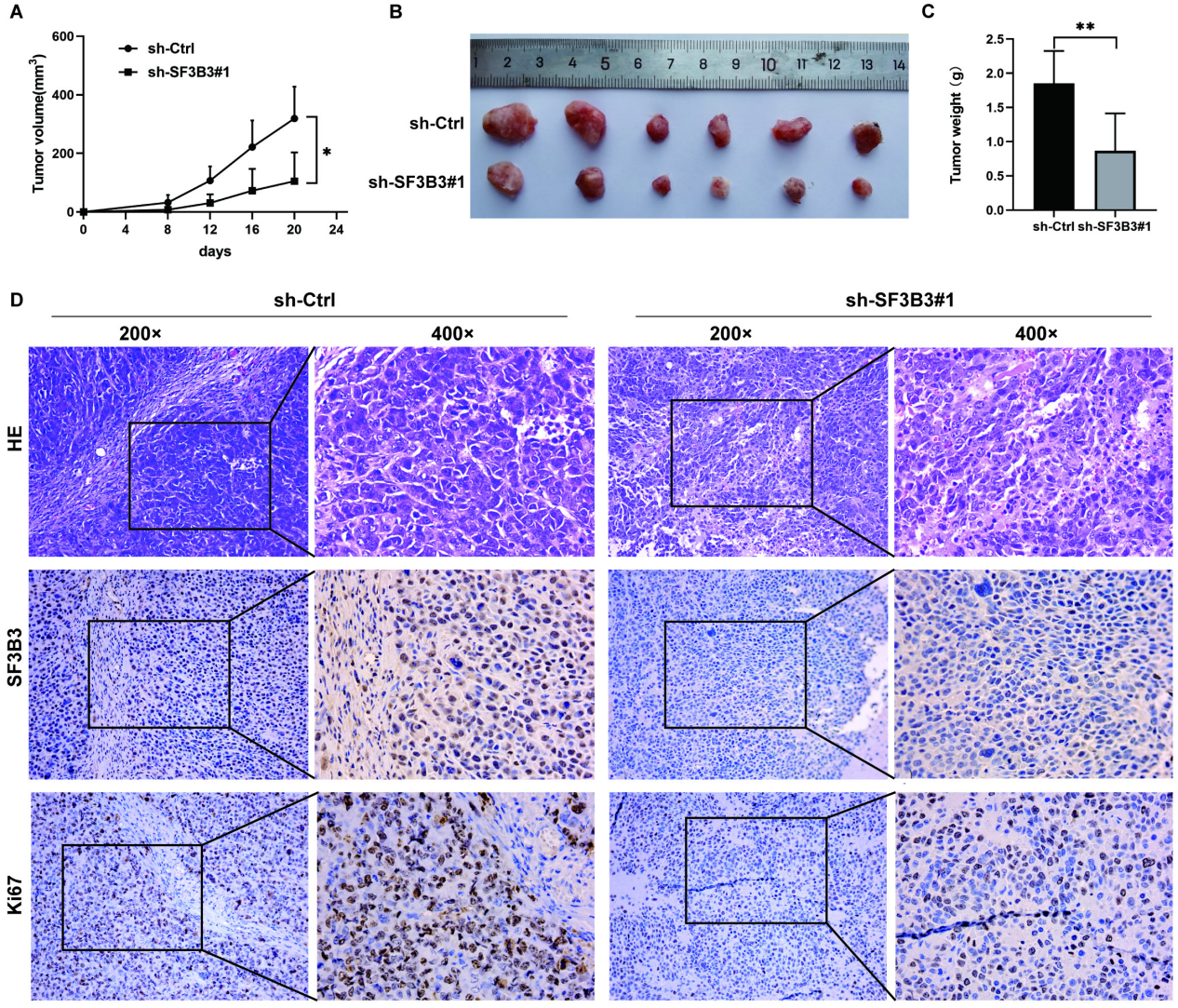

Figure 3. The impact of SF3B3 on the growth of gastric cancer xenografts. A) Morphological comparison of xenografts with knockdown of SF3B3 (sh-SF3B3) and controls (sh-Ctrl); B) Changes in xenograft volume; C) Changes in xenograft weight; D) H&E and immunohistochemical (SF3B3 and Ki-67 proteins) staining. n=6. **p<0.01

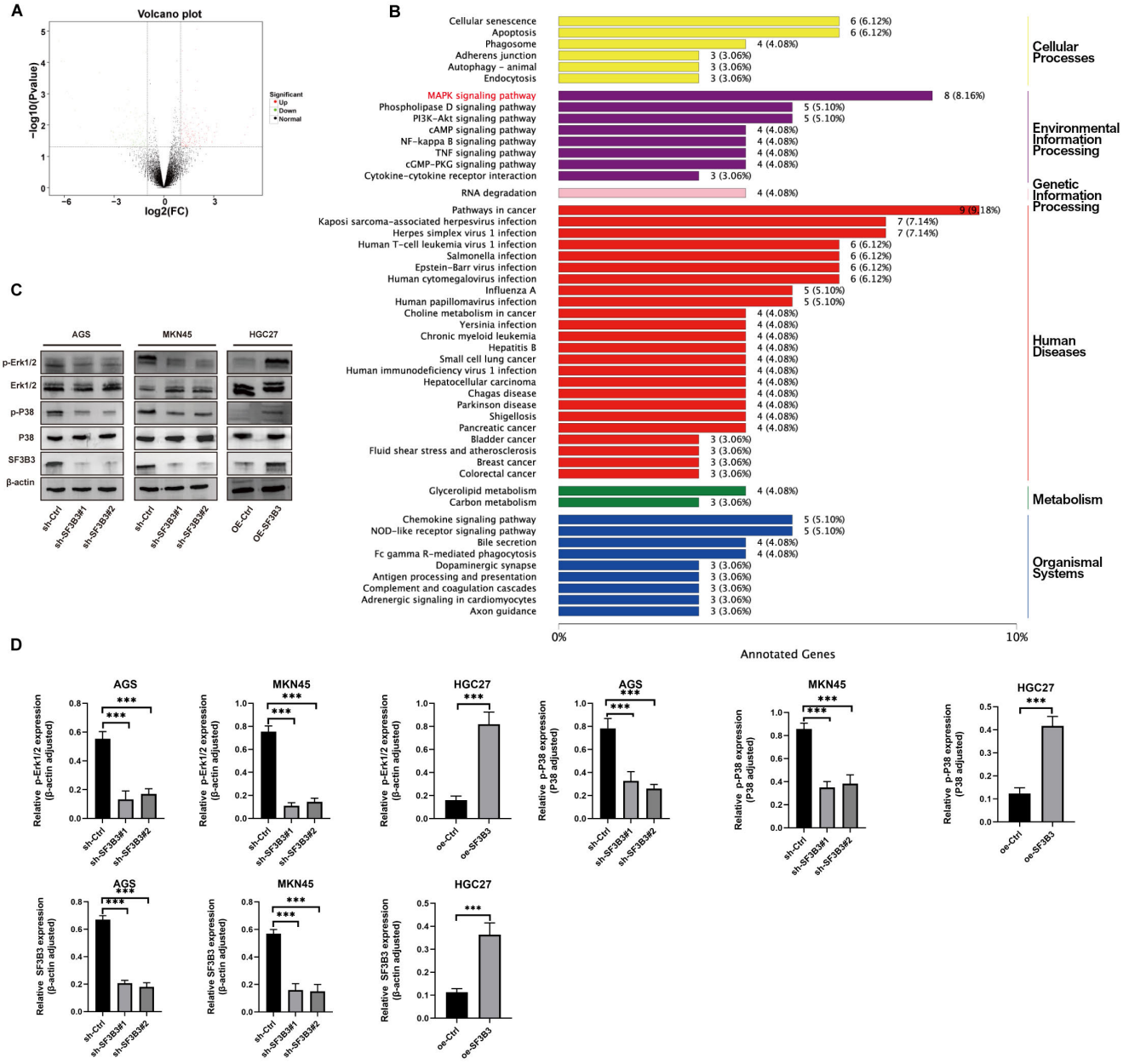

Figure 4. The impact of SF3B3 on the ERK/MAPK P38 signaling pathway in gastric cancer cells. A) Volcano plot of differentially expressed mRNA (transcriptome analysis); B) KEGG enrichment analysis of differential genes; C, D) Western blot experiments to detect proteins related to the ERK/MAPK P38 signaling pathway (C), and semi-quantitative analysis (D). n=3, ***p<0.001

that the transcription factor ELK1 could regulate the expression of the SF3B3 gene across all three databases (Figure 5A). Concurrently, online databases were utilized to discover a significant positive correlation between SF3B3 expression and ELK1 (Figure 5B). Overexpression of ELK1 in 293T and MKN45 cells significantly increased the expression of SF3B3 (Figure 5C, Supplementary Figure S4A). Furthermore, based on the predicted ELK1 binding to the P5 segment of the SF3B3 promoter sequence from the Jaspar database, ChIP experiments were conducted, which found that the P5 sequence could be significantly bound and precipitated by ELK1 in 293T and MKN45 cells (Figures 5D, 5E, Supplementary Figure S4B). A dual-luciferase reporter assay was performed using a construct with the P5 sequence, further confirming that ELK1 could significantly enhance the expression of firefly luciferase by binding to the P5 sequence in the promoter region of the SF3B3 gene in 293T and MKN45 cells (Figure 5F, Supplementary Figure S4C).

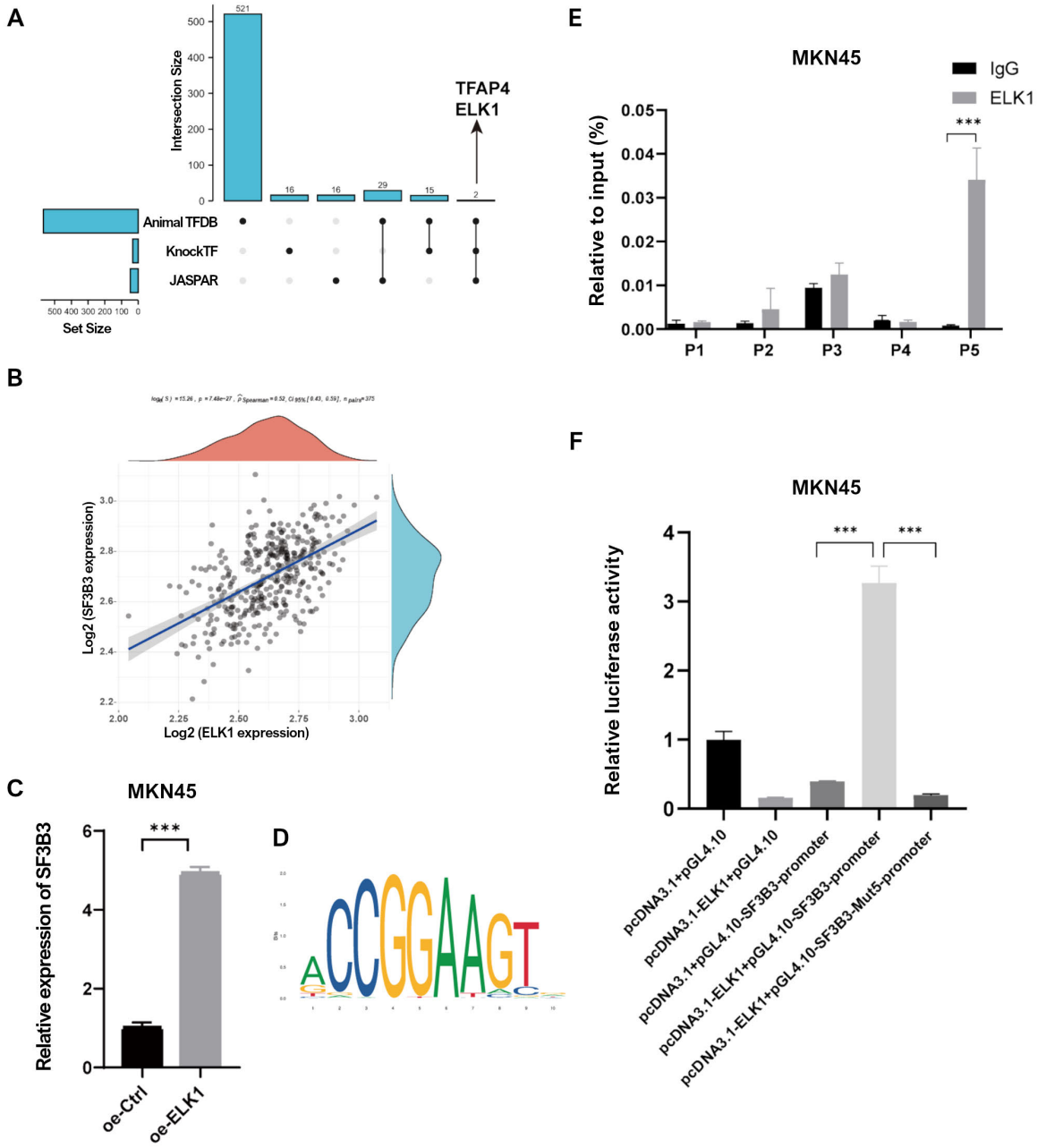

Figure 5. The regulatory effect of the ELK1 transcription factor on the expression of the SF3B3 gene. A) Analysis of transcription factors for the SF3B3 gene in the AnimalTFDB, KnockTF, and JASPAR online databases; B) Analysis of the correlation between SF3B3 and ELK1 expression using TCGA online database; C) qPCR detection of the effect of overexpressing ELK1 on SF3B3 expression in MKN45 cells; D) Prediction of the binding region P1-P5 of the transcription factor ELK1 on the SF3B3 gene promoter from the JASPAR database; E, F) ChIP (E) and dual-luciferase assay (F) to verify the binding region of ELK1 on the SF3B3 gene promoter. n=3, ***p<0.001

Discussion

RNA splicing is closely related to cell proliferation, survival, and differentiation, and is implicated in many human cancers. Studies have shown that in lymphoma, MYC can directly induce the transcription of snRNP genes and the arginine methyltransferase PRMT5, whose substrate is a component of the RNA splicing machinery [14, 15]. Several tumor suppressor genes, such as PTEN, ARID1A, and CDKN1A, are inactivated or downregulated at the transcriptional level due to aberrant AS, leading to the retention of introns [16, 17]. Additionally, aberrant AS in tumors can produce 12 protein isoforms of TP53, which are either inactivated due to intron retention or bind to different gene

promoters, leading to abnormal transcriptional regulation and promoting cellular transformation [18]. Therefore, elucidating the role of AS in cancer development is crucial for uncovering new targets for cancer therapy.

SF3B3 is a subunit of the splicing factor 3B complex (SF3B), which, together with SF3A and the 12S RNA unit, forms the U2 small nuclear ribonucleoprotein complex (U2 snRNP), a key nucleophile in the first transesterification reaction of the splicing reaction. Multiple studies have found that SF3B3 promotes the occurrence and development of various cancers, including colon, bladder, ovarian, breast, and liver cancer [18–21]. This study, through analysis of TCGA database, found that SF3B3 expression was significantly elevated in GC tissues, and patients with high SF3B3 expression had poorer prognosis, suggesting that SF3B3 may promote GC, potentially through aberrant high expression leading to dysregulation of AS. This finding is consistent with previous results, further confirming the important role of SF3B3 in GC. This study further reveals that SF3B3 is closely related to the immune microenvironment of GC. Its expression levels are significantly positively correlated with the infiltration of Th2 cells, T helper cells, and NK CD56 bright cells, and significantly negatively correlated with the infiltration of Tgd, TFH, T cells, pDC cells, NK cells, mast cells, macrophages, iDC cells, DC cells, cytotoxic cells, CD8 T cells, and B cells. These immune cells can interact with each other and synergistically promote the immune escape of GC. Immune escape can further promote the proliferation and metastasis of tumor cells. To this end, this study has verified the impact of SF3B3 on the proliferation, metastasis, and growth of GC *in vitro* and *in vivo* experiments. Further *in vitro* experiments revealed that knockdown of SF3B3 significantly inhibited the proliferation, colony formation, migration, and invasion of GC cells, while inducing apoptosis and cell cycle arrest. Interestingly, SF3B3 silencing in GC cells increased the S-phase fraction yet simultaneously reduced EdU fluorescence intensity. In normally proliferating cells, an expanded S-phase population typically signifies robust proliferation and thus higher EdU incorporation. Here, however, the S-phase accumulation resulted from S-phase arrest rather than accelerated progression, impairing DNA replication and consequently diminishing EdU incorporation during the last 2 h of cell cultivation. Consistent with this interpretation, Cyclin D1 and Cyclin A levels were downregulated in sh-SF3B3 cells. To validate this observation, dual-parameter flow cytometry combining Hoechst 33342 with EdU-Apollo643 will be performed in subsequent experiments. In contrast, overexpression of SF3B3 promoted these cellular behaviors, indicating that SF3B3 plays a significant role in promoting the proliferation and invasion of GC cells.

Current research on the downstream molecular mechanisms by which SF3B3 regulates cancer development is relatively clear, and it is based on the aberrant selective splicing of target genes by SF3B3 to promote carcinogenesis. In renal cancer, SF3B3 may have potential oncogenic effects through the selective splicing of EZH2 pre-mRNA [22]. In liver cancer, LINC01348 can prevent cancer cell metastasis by inhibiting SF3B3-mediated selective splicing of EZH2 pre-mRNA [19]. In colon cancer, SF3B3-mediated selective splicing of mTOR pre-mRNA promotes the progression and metastasis of rectal cancer [18]. This study found that SF3B3 can promote the proliferation and inhibit apoptosis of GC cells by activating the MAPK pathway, providing a new perspective on the role of SF3B3 in GC. However, whether it forms new structures of persistently activated MAPK proteins through selective splicing requires further investigation. Despite this, the mechanisms by which aberrant SF3B3 is regulated in cancer are unclear. As a culprit in the transformation of multiple genes into oncogenes, understanding the molecular mechanisms leading to its aberrance is of great significance. This study found that the ELK1 transcription factor can regulate the expression of SF3B3, and there is a significant positive correlation between SF3B3 and ELK1. Overexpression of ELK1 in 293T and MKN45 cells significantly increased the expression of SF3B3. This discovery reveals a new mechanism for the regulation of SF3B3 expression and provides a new molecular target for GC therapy.

In summary, this study not only confirms the important role of SF3B3 in GC but also reveals its molecular mechanisms in regulating GC proliferation and apoptosis, which may be closely related to the ELK1-SF3B3-MAPK signaling axis. This provides new targets for the precision treatment of GC and has the potential to improve the prognosis of GC patients. Future research can further explore the other functions and mechanisms of SF3B3 in GC, as well as the potential applications of the ELK1-SF3B3-MAPK signaling axis in GC therapy.

Supplementary information is available in the online version of the paper.

Acknowledgments: This work was supported by the National Natural Science Foundation of China (No. 82473266); Key Talents Project of Gansu Province (No. 2019RCXM020); Gansu Province Innovation Driven Assistance Project (No. GXH20230817-14); Cuiying Scientific and Technological Innovation Program of Lanzhou University Second Hospital (No. CY2023-ZD-01); Natural Science Foundation of Gansu province (No. 22JR5RA721).

References

[1] YANG WJ, ZHAO HP, YU Y, WANG JH, GUO L et al. Updates on global epidemiology, risk and prognostic factors of gastric cancer. World J Gastroenterol 2023; 29: 2452–2468. https://doi.org/10.3748/wjg.v29.i16.2452

[2] VINCZE Á. Endoscopic diagnosis and treatment in gastric cancer: Current evidence and new perspectives. Front Surg 2023; 10: 1122454. https://doi.org/10.3389/fsurg.2023.1122454

[3] SMYTH EC, NILSSON M, GRABSCH HI, VAN GRIEKEN NCT, LORDICK F. Gastric cancer. Lancet 2020; 396: 635–648. https://doi.org/10.1016/S0140-6736(20)31288-5

[4] ZHANG Y, QIAN J, GU C, YANG Y. Alternative splicing and cancer: a systematic review. Signal Transduct Target Ther 2021; 6: 78. https://doi.org/10.1038/s41392-021-00486-7

[5] WANG TY, LIU Q, REN Y, ALAM SK, WANG L et al. A pan-cancer transcriptome analysis of exitron splicing identifies novel cancer driver genes and neoepitopes. Mol Cell 2021; 81: 2246–2260.e2212. https://doi.org/10.1016/j.molcel.2021.03.028

[6] DENG K, YAO J, HUANG J, DING Y, ZUO J. Abnormal alternative splicing promotes tumor resistance in targeted therapy and immunotherapy. Transl Oncol 2021; 14: 101077. https://doi.org/10.1016/j.tranon.2021.101077

[7] SCIARRILLO R, WOJTUSZKIEWICZ A, ASSARAF YG, JANSEN G, KASPERS GJL et al. The role of alternative splicing in cancer: From oncogenesis to drug resistance. Drug Resist Updat 2020; 53: 100728. https://doi.org/10.1016/j.drup.2020.100728

[8] PENG Q, ZHOU Y, OYANG L, WU N, TANG Y et al. Impacts and mechanisms of alternative mRNA splicing in cancer metabolism, immune response, and therapeutics. Mol Ther 2022; 30: 1018–1035. https://doi.org/10.1016/j.ymthe.2021.11.010

[9] LI Y, DIAO Y, WANG Z, WANG S, PENG J et al. The splicing factor SF3B4 drives proliferation and invasion in cervical cancer by regulating SPAG5. Cell Death Discov 2022; 8: 326. https://doi.org/10.1038/s41420-022-01120-3

[10] SUN C. The SF3b complex: splicing and beyond. Cell Mol Life Sci 2020; 77: 3583–3595. https://doi.org/10.1007/s00018-020-03493-z

[11] GÖKMEN-POLAR Y, NEELAMRAJU Y, GOSWAMI CP, GU X, NALLAMOTHU G et al. Expression levels of SF3B3 correlate with prognosis and endocrine resistance in estrogen receptor-positive breast cancer. Mod Pathol 2015; 28: 677–685. https://doi.org/10.1038/modpathol.2014.146

[12] HÄNZELMANN S, CASTELO R, GUINNEY J. GSVA: gene set variation analysis for microarray and RNA-seq data. BMC Bioinformatics 2013; 14: 7. https://doi.org/10.1186/1471-2105-14-7

[13] BINDEA G, MLECNIK B, TOSOLINI M, KIRILOVSKY A, WALDNER M et al. Spatiotemporal dynamics of intratumoral immune cells reveal the immune landscape in human cancer. Immunity 2013; 39: 782–795. https://doi.org/10.1016/j.immuni.2013.10.003

[14] HODSON DJ, SCREEN M, TURNER M. RNA-binding proteins in hematopoiesis and hematological malignancy. Blood 2019; 133: 2365–2373. https://doi.org/10.1182/blood-2018-10-839985

[15] KOH CM, BEZZI M, LOW DHP, ANG WX, TEO SX et al. MYC regulates the core pre-mRNA splicing machinery as an essential step in lymphomagenesis. Nature 2015; 523: 96–100. https://doi.org/10.1038/nature14351

[16] LUO J, SOLIMINI NL, ELLEDGE SJ. Principles of cancer therapy: oncogene and non-oncogene addiction. Cell 2009; 136: 823–837. https://doi.org/10.1016/j.cell.2009.02.024

[17] TARN WY, STEITZ JA. A Novel Spliceosome Containing U11, U12, and U5 snRNPs Excises a Minor Class (AT–AC) Intron In Vitro. Cell 1996; 84: 801–811. https://doi.org/10.1016/S0092-8674(00)81057-0

[18] XU T, LI X, ZHAO W, WANG X, JIN L et al. SF3B3-regulated mTOR alternative splicing promotes colorectal cancer progression and metastasis. J Exp Clin Cancer Res 2024; 43: 126. https://doi.org/10.1186/s13046-024-03053-4

[19] LIN YH, WU MH, LIU YC, LYU PC, YEH CT et al. LINC01348 suppresses hepatocellular carcinoma metastasis through inhibition of SF3B3-mediated EZH2 pre-mRNA splicing. Oncogene 2021; 40: 4675–4685. https://doi.org/10.1038/s41388-021-01905-3

[20] ZHANG S, ZHANG J, AN Y, ZENG X, QIN Z et al. Multi-omics approaches identify SF3B3 and SIRT3 as candidate autophagic regulators and druggable targets in invasive breast carcinoma. Acta Pharm Sin B 2021; 11: 1227–1245. https://doi.org/10.1016/j.apsb.2020.12.013

[21] GÖKMEN-POLAR Y, NEELAMRAJU Y, GOSWAMI CP, GU X, NALLAMOTHU G et al. Expression levels of SF3B3 correlate with prognosis and endocrine resistance in estrogen receptor-positive breast cancer. Mod Pathol 2015; 28: 677–685. https://doi.org/10.1038/modpathol.2014.146

[22] CHEN K, XIAO H, ZENG J, YU G, ZHOU H et al. Alternative Splicing of EZH2 pre-mRNA by SF3B3 Contributes to the Tumorigenic Potential of Renal Cancer. Clin Cancer Res 2017; 23: 3428–3441. https://doi.org/10.1158/1078-0432.ccr-16-2020

https://doi.org/10.4149/neo_2025_250219N83

ELK1 modulates SF3B3 transcriptional activity to stimulate proliferation and inhibit apoptosis in gastric cancer through the activation of the MAPK pathway

Yaqing ZHANG[1,#], Lei GAO[1,#], Lixin LIU[2], Hao CHEN[1,3,4,*]

Supplementary Information

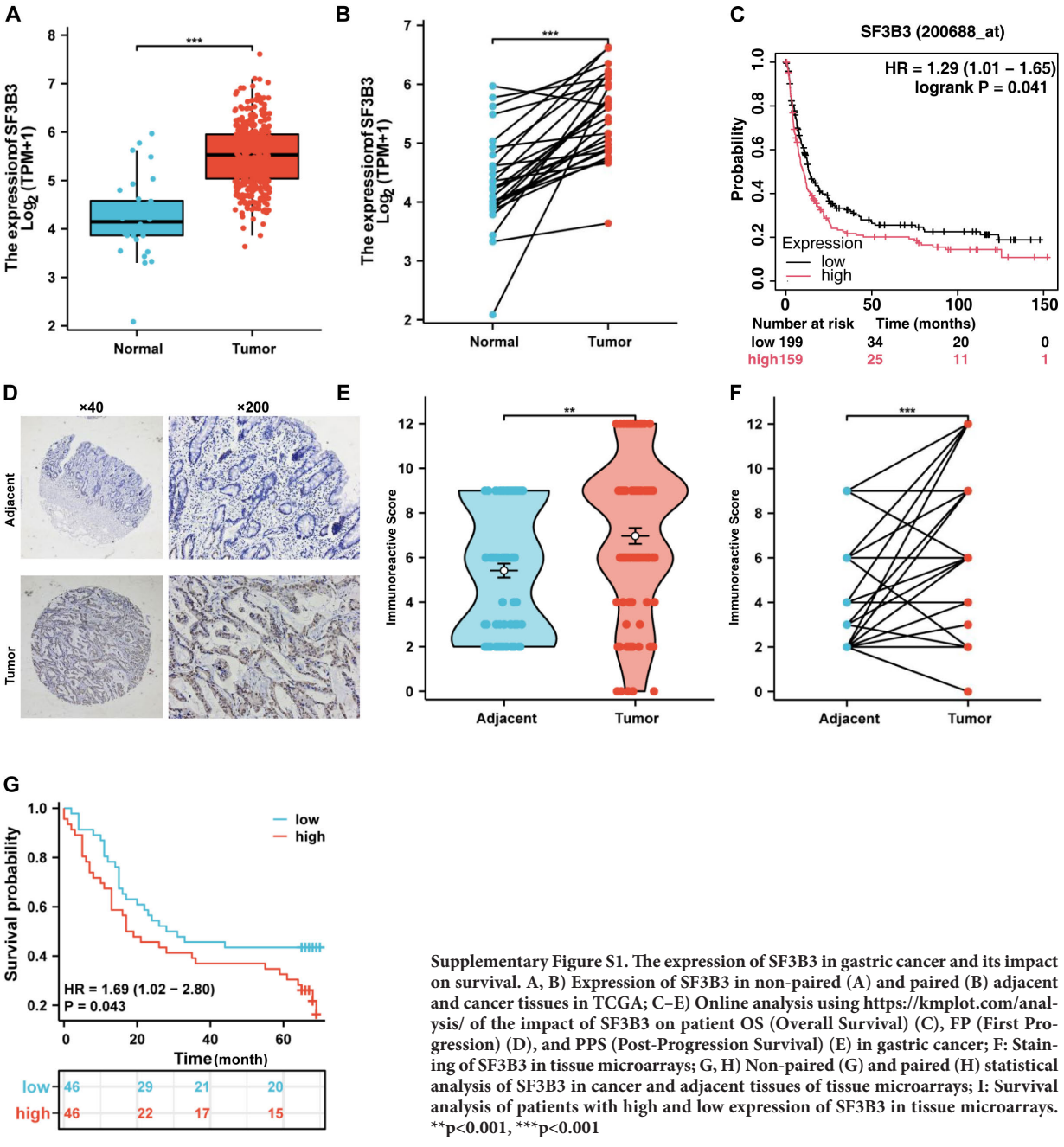

Supplementary Figure S1. The expression of SF3B3 in gastric cancer and its impact on survival. A, B) Expression of SF3B3 in non-paired (A) and paired (B) adjacent and cancer tissues in TCGA; C–E) Online analysis using https://kmplot.com/analysis/ of the impact of SF3B3 on patient OS (Overall Survival) (C), FP (First Progression) (D), and PPS (Post-Progression Survival) (E) in gastric cancer; F: Staining of SF3B3 in tissue microarrays; G, H) Non-paired (G) and paired (H) statistical analysis of SF3B3 in cancer and adjacent tissues of tissue microarrays; I: Survival analysis of patients with high and low expression of SF3B3 in tissue microarrays. **p<0.001, ***p<0.001

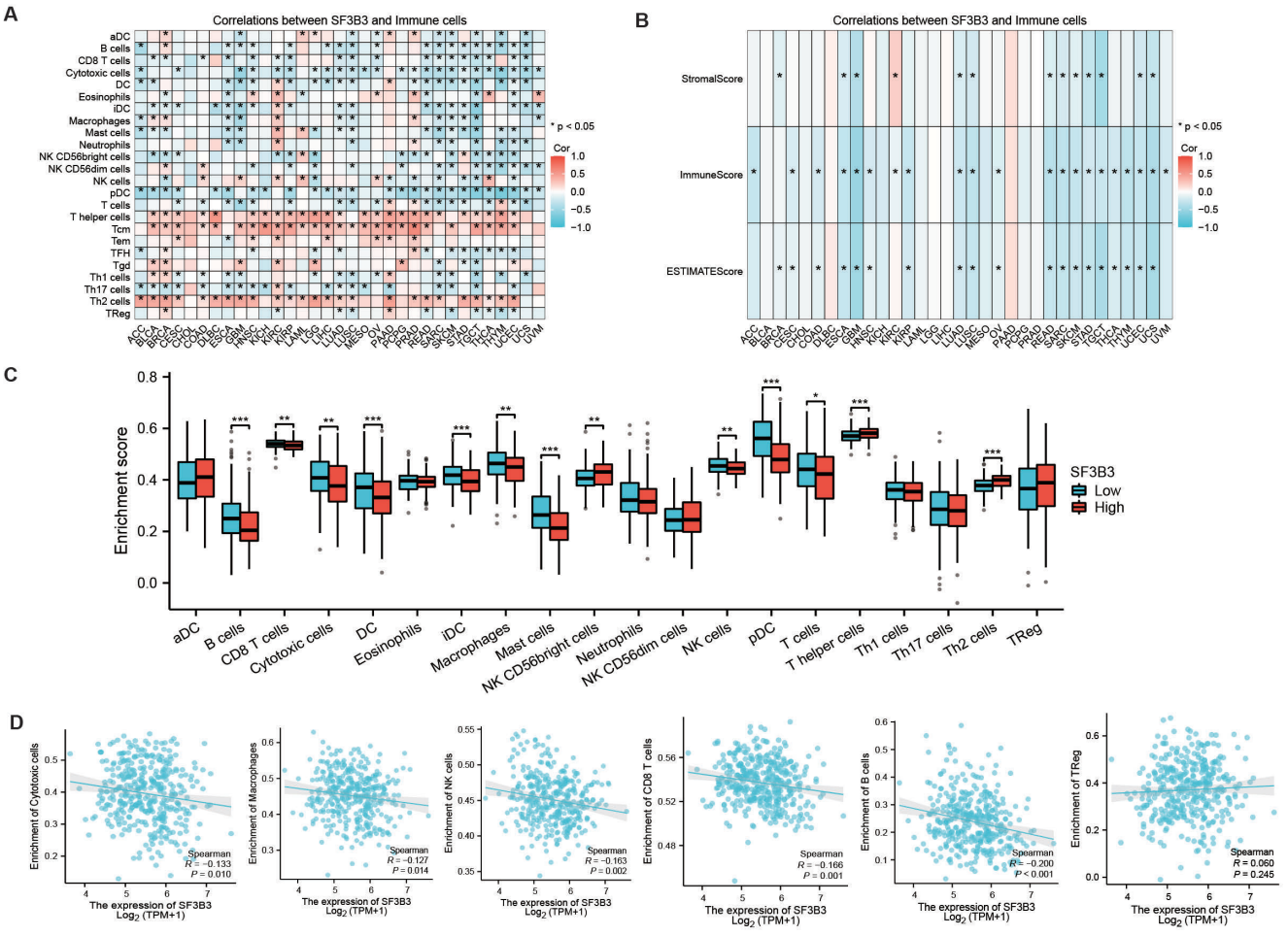

Supplementary Figure S2. The Relationship between SF3B3 Expression and Immune Infiltration. A) Correlation between SF3B3 and immune cells; the color represents the correlation coefficient (Cor), with red indicating a positive correlation and blue indicating a negative correlation. The intensity of the color reflects the strength of the correlation. *p<0.05. B) The relationship between SF3B3 gene expression and stromal score (StromalScore), immune score (ImmuneScore), and ESTIMATE score. The color represents the correlation coefficient (Cor), with red indicating a positive correlation and blue indicating a negative correlation. The intensity of the color reflects the strength of the correlation. *p<0.05. C) Enrichment scores of different immune cells in groups with high and low SF3B3 expression. *p<0.05, **p<0.01, ***p<0.001. D) The correlation between SF3B3 expression and the enrichment of different immune cells, with Spearman correlation coefficients (R) and p-values indicating the strength and significance of the correlation.

Supplementary Table S1. Primer sequences.

SF3B3 gene		Detailed information of primer sequences
Specific primer P1	F	5'-CTTCGTTGGCGCCTATTTGG-3'
	R	5'-ATGCTTCCGTCTTGCTTCCA-3'
Specific primer P2	F	5'-AATCAACGGGGGTCTAGGGA-3'
	R	5'-TCTCCTTGCTGGGGGATACA-3'
Specific primer P3	F	5'-CCCACAGAAGTGCCCAATGA-3'
	R	5'-ATGCTTCCGTCTTGCTTCCA-3'
Specific primer P4	F	5'-GTCTGGGAAACAGCTGACAAG-3'
	R	5'-TTTTCAGTGGCAACTCGATGCT-3'
Specific primer P5	F	5'-TGAGCTCAGCGGAGATTTCG-3'
	R	5'-CCAAATAGGCGCCAACGAAG-3'

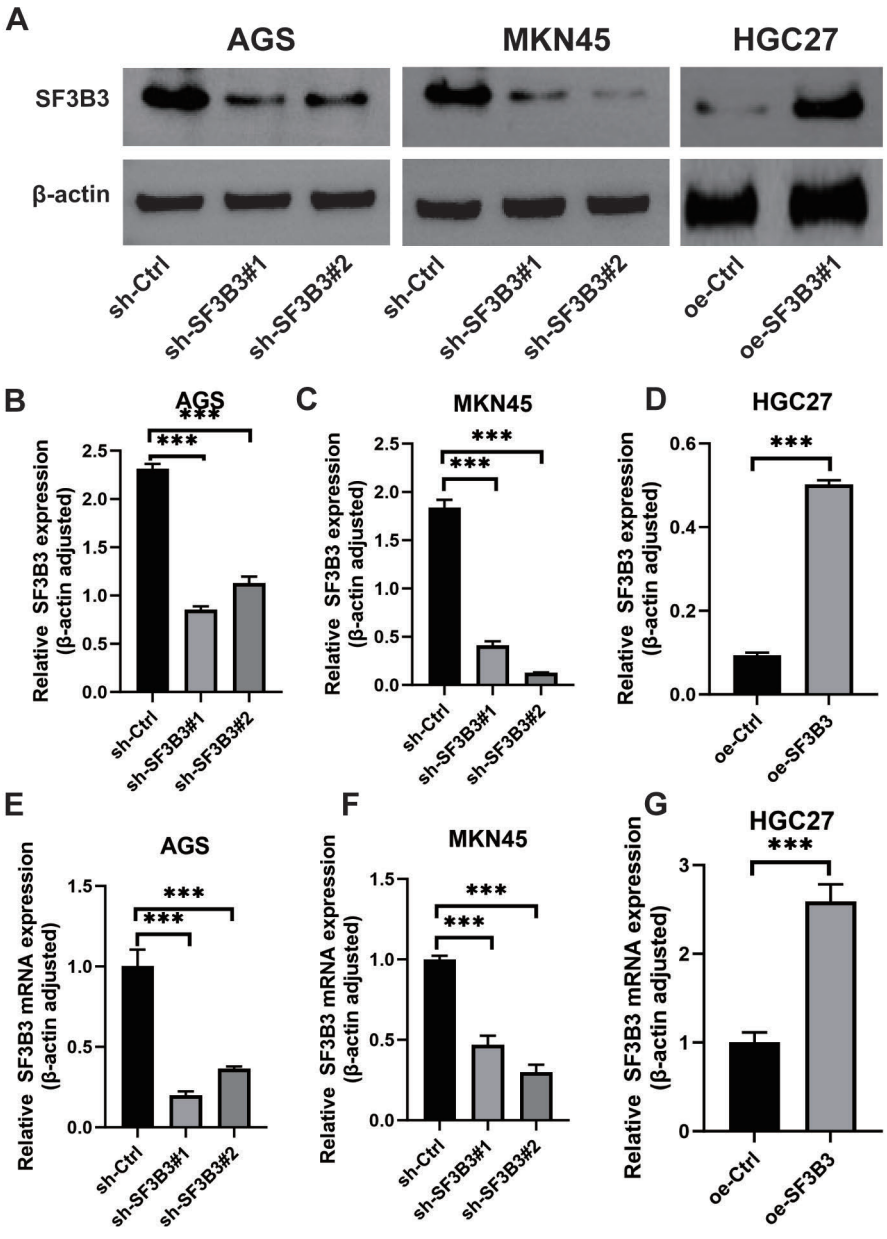

Supplementary Figure S3. Validation of SF3B3 Gene Knockdown and Overexpression efficiency. A) Western blot analysis validating the knockdown efficiency of SF3B3 in AGS and MKN45 cells and the overexpression efficiency in HGC27 cells. B–C: Statistical analysis of band intensity quantification from the Western blot assay. D–E) qPCR validation of SF3B3 mRNA expression efficiency. n=3. *p<0.05, **p<0.01, ***p<0.001

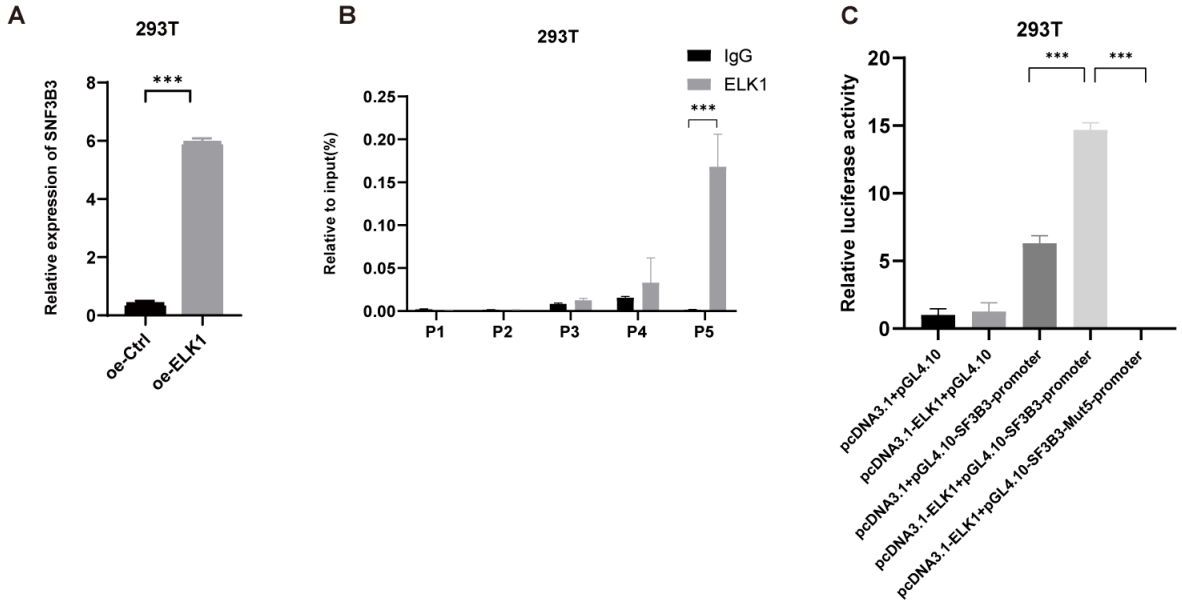

Supplementary Figure S4. The regulatory effect of the ELK1 transcription factor on the expression of the SF3B3 gene in 293T cells. A) qPCR detection of the effect of overexpressing ELK1 on SF3B3 expression in 293T cells; B, C) CHIP (B) and dual-luciferase assay (C) to verify the binding region of ELK1 on the SF3B3 gene promoter. n=3, ***p<0.001